Ocean Engineering 189 (2019) 106409

Contents lists available at ScienceDirect

Ocean Engineering

journal homepage: www.elsevier.com/locate/oceaneng

Distribution of wave heights on steep submerged reefs

Thieu Quang Tuan [a,*], Dinh Quang Cuong [b]

[a] Faculty of Marine and Coastal Engineering, Thuy Loi University (TLU), 175 Tay Son, Dong Da District, Hanoi, Viet Nam
[b] Institute of Construction for Offshore Engineering, National University of Civil Engineering, 55 Giai Phong, Ba Dinh District, Hanoi, Viet Nam

ARTICLE INFO

Keywords:
Wave height distribution
Weibull
Platform reefs
Reef flat
Wave breaking

ABSTRACT

Extensive laboratory experiments were carried out to investigate the statistical characteristics of wave heights on steep submerged (platform) reefs. Compared with the situation on a gently-sloping beach, the extraordinary wave breaking induced by abrupt depth reduction over a steep fore-reef slope makes the wave height distribution on the reef flat to differ substantially. Existing models of wave height distributions on shallow beaches such as by Battjes and Groenendijk (2000) thus come out to be less reliable. To resolve this, a new composite Weibull distribution model has been proposed and formulated based on 540 measured wave records at various locations across the reef flat. The model is generally composed out of three Weibull parts and collapses to a two-Weibull distribution in a situation of low relative wave energy. The newly-proposed model shows good predictive capacity on most common characteristic wave heights in comparison with the present and several existing laboratory datasets.

1. Introduction

Wave height distributions in shallow coastal water are essential for determining design wave heights and subsequently design wave forcing on coastal structures. Likewise, the distribution of wave heights on offshore submerged (platform) reefs is also needed, for example, to resolve design impact loads induced by wave breaking on structures located on the reef flat tops.

Deep-water wave heights are theoretically shown to obey the Rayleigh distribution (Longuet-Higgins, 1952). In shallow water, shoaling, nonlinear interactions and most importantly depth-induced wave breaking make the wave height distribution to differ significantly from the theoretical Rayleigh form. In this context, it is common to address wave breaking to occur on a gentle beach (say slope less than 1/20) with gradual depth variation. However, in the case on a submerged reef considered herein waves also break as the water depth suddenly reduces to a breaking limit on the reef flat. The abrupt depth transition over a steep reef (the fore-reef slope is typically between 1/15 and 1/5) results in unordinary breaking conditions, wave transformation and consequently the distribution of wave heights on the reef flat therefore might noticeably deviate from those ordinary on a shallow beach. For clarity, characteristics of wave breaking and wave hydrodynamics on steep reefs are briefly reviewed in the following.

Nelson (1994) noted that the maximum individual wave height to water depth ratio at locations behind the reef-edge surfzone on a horizontal reef flat should not exceed 0.55, far below the commonly accepted value of 0.80. In a laboratory investigation on regular wave transformation on a fringing reef, Gourlay (1994) noticed that wave breaking conditions on the reef edge are substantially different from those on a plane beach. The wave transmission regime is classified according to a non-linearity parameter representing wave conditions at the reef edge. The maximum wave height to depth ratio on the reef flat is found to depend on this non-linearity parameter and turns out to be consistent with the finding by Nelson (1994) for a horizontal bed. Yao et al. (2013) experimentally examined characteristics of breaking of monochromatic waves on fringing reefs with various fore-reef slopes. The results reveal that most of the wave breaking features over the reef such as breaker types and breaker indices are mainly characterized by the relative reef-flat submergence (i.e. the ratio of the water depth over the reef flat d to the offshore incident wave height $H_{m0,0}$, $d/H_{m0,0}$), but not by the surf similarity like on plane beaches (Battjes, 1974).

Besides wave breaking, a vast number of field and laboratory studies exist in the literature on the reef wave dynamics (see e.g. Nakaza and Hino, 1991; Lowe et al., 2005; Demirbilek et al., 2007; Nwogu and Demirbilek, 2010; Buckley et al., 2015; Becker et al., 2016; Buckley et al., 2018). Collectively, these describe the two important hydrodynamic features on reefs that are low-frequency motions or infra-gravity waves (frequencies $f < 0.04$ Hz in field scales, henceforth designated as

* Corresponding author.
E-mail address: Tuan.T.Q@tlu.edu.vn (T.Q. Tuan).

https://doi.org/10.1016/j.oceaneng.2019.106409
Received 1 December 2018; Received in revised form 16 August 2019; Accepted 3 September 2019
Available online 25 September 2019

IG waves) and the super-elevated water level (wave setup). In steep reef environments, their magnitudes can potentially be enhanced compared to those on open gentle beaches. Wave setup and low-frequency motions can be major components of wave run-up at a reef-fringed shoreline.

Wave setup on steep reefs can be very significant due to large gradients of the cross-shore radiation stress as the result of abrupt depth-reduction-induced wave breaking around the reef edge (Buckley et al., 2015) and thus is primarily influenced by the water depth over the reef. Wave setup generally increases with a decrease in the relative reef-flat submergence (see e.g. Gourlay, 1996a; 1996b). Higher bottom roughness also tends to increase setup through its effects on the bottom stress in the across-shore momentum balance. The influence of higher roughness on setup, however, can partially be cancelled out by the effect of reduced wave heights due to increased frictional wave dissipation (Buckley et al., 2016). Wave setup is also affected by the reef profile features. Setup on a platform reef (considered in this study), where water is able to escape leeward, is considerably less than that on a fringing reef (see e.g. Gourlay, 1996a; 1996b). Nevertheless, the effect of wave setup on wave heights can straightforwardly be incorporated through including setup in the mean water level (allowing for larger wave heights to exist on the reef flat). In this study, the effect of wave setup on the wave height distribution is implicit in the measured wave heights across the reef.

IG waves on a steep reef are predominantly generated by breaking processes of short-period waves around the reef-edge, i.e. oscillation of the breakpoint mechanism (see e.g. Pomeroy et al., 2012; Becker et al., 2016; Buckley et al., 2018). As short-period waves dissipate due to breaking the relative importance of IG waves start to increase toward the shore and can even dominate near the shoreline or inside the lagoon behind reefs. Also, resonant amplification of standing IG waves can potentially occur, leading to a notable increase in wave run-up (Nakaza and Hino, 1991; Péquignet et al., 2009; Nwogu and Demirbilek, 2010; Pomeroy et al., 2012; Buckley et al., 2018; Yao et al., 2019). Eventual effects of IG waves on the wave height statistics are not straightforward and further discussed in Section 5.

Despite the noticeable difference in wave hydrodynamics, published research has not been available yet for the wave height distribution on submerged reefs. In terms of explicitness and ease of application, models for the wave height distribution with the effect of wave breaking can be split into two groups. First is those largely rely on theoretical approximations (Tayfun, 1981) or purely algorithmic manipulations (see e.g. Mase and Iwagaki, 1982; Dally and Dean, 1986) and therefore are either impractical or implicit for use in engineering applications. In the second and most popular group empirical distributions such as Weibull are adopted, whereby model parameters can straightforwardly be formulated with experimental data (see e.g. Glukhovskiy, 1966; Klopman, 1996; Battjes and Groenendijk, 2000; Rattanapitikon, 2010; Wu et al., 2016). In the present study we also advocate the second approach and a review on most relevant studies with consideration of wave breaking effects is given in the following.

Glukhovskiy (1966, see Bouws, 1979) extended the Rayleigh distribution for wave heights in finite water depth through explicit inclusion of the wave height to water depth ratio H_s/d as the model breaker parameter. Klopman (1996) further modified the Glukhovskiy distribution to a more consistent Weibull distribution with two distinct parameters. However, at hinted at by the fact that the distribution by Klopman (1996) still overestimates extreme wave heights while underestimates lower ones, Battjes and Groenendijk (2000) arrived at a composite Rayleigh-Weibull distribution (henceforth referred to as the BG2000). The two parts of the BG2000 distribution are joined at a transitional wave height. The upper distribution (i.e. above the transitional wave height) is particularly for high waves affected by depth-limited conditions. Laboratory data of wave heights on various beach slopes ranging from 1/20 to 1/250 were used to formulate the model parameters as functions of local spectral wave energy (m_0), water depth and bottom slope. Also, the breaker parameter known as the relative wave intensity or wave saturation degree represented by $\sqrt{m_0}/d$ is used instead of H_s/d in the model.

The approach of composite distributions by Battjes and Groenendijk (2000) is considered most suitable for wave heights in shallow water and thus has been pursued in numerous laboratory and field studies on the model verification and validation. Herein, without loss of generality, more attention is therefore paid to the BG2000 model.

Mai et al. (2010) showed a consistent underestimation of high waves by the BG2000 model compared with field data along the German coast, recommending amendments of both the transitional wave height and the exponent of the upper distribution. In a situation of low relative wave intensity, Caires and van Gent (2012) also reported that estimates of $H_{0.1\%}$ by the BG2000 model are as much as 15% lower than laboratory (broken waves) and field data (lake waves) of wave heights on flat bottoms. On the contrary, Christou et al. (2011) spotted that both the BG2000 and Glukhovskiy (1966) models largely over-predict their measurements collected at Duck field experiment site (North Carolina, USA).

Comparisons of the BG2000 model with laboratory measurements also report the same discrepancies. Vasiliki and Swan (2011) found the model largely over-estimates their largest wave heights on mild beach slopes at shallowest locations, while Vledder (2013) showed the opposite when comparing with data of wave heights on a barred beach by Boers (1996).

Rattanapitikon (2010) attempted to verify seventeen conversion formulas for several representative wave heights derived from existing and modified distributions against large existing (laboratory and field) datasets covering a wide range of wave conditions from deep to shallow water. Since the study mainly focused on the overall predictive performances of the formulations, but not on detailed agreements of the considered distributions themselves, no insight into the existing models with regards to the effect of wave breaking was given.

The contradicting results amongst the aforementioned model comparisons might be attributed to factors that are inadequately addressed by the existing models such as bottom topographic conditions, the local spectral shape (influenced by the foreshore shallowness, see Hofland et al., 2017), or even the number of waves considered. It generally follows that the existing distributions including that by Battjes and Groenendijk (2000) work reasonably well in intermediate water, while in shallower depths discrepancy arises for highest waves, i.e. at the tail. Also, it is noticed that the trend of measured data and the shape of the distribution at the tail of the Weibull part are largely dissimilar, overall agreement of the BG2000 model therefore cannot be achieved simply through tuning the model parameters. Wu et al. (2016) argued that wave heights in shallow water are limited by the breaking criteria so that the Weibull tail without an upper limit seems inappropriate. The authors therefore proposed a new composite Weibull-generalised Pareto distribution, in which the transitional wave height between the two parts is set at the significant wave height H_s and the breaking criteria by Miche (1944) is used as the upper limit. Though the limit is rather theoretical the model was claimed to perform well for the wave height distribution as a whole under various wave conditions from deep to shallow water. However, as the study did not particularly aim at depth-induced breaking waves and only a few datasets of breaking waves were available, the model performance for the tail in cases with wave breaking was not evidenced. In this regard, the distribution by Glukhovskiy (1966) was found the best.

It is emphasized that all of the considered existing distributions were not fitted with individual wave heights from measured records, but with datasets of representative wave heights only (i.e. at $H_{1/3}$, H_m, $H_{1\%}$, $H_{0.1\%}$, etc.).

In the present study context, it appears that both in terms of adaptability and of simplicity the model approach by Battjes and Groenendijk (2000) is most attractive. The study goal is therefore to extend the model approach by Battjes and Groenendijk (2000) to better describe the wave height distribution on submerged reefs. To this end, laboratory

experiments of wave transformation across submerged reefs are conducted, whereby the proposed model can be parameterized with all individual wave heights.

2. Laboratory experiments

The scale model experiments were conducted in the 45 m long and 1.0 m wide wave flume of Thuy Loi University, Hanoi, Vietnam (formerly Water Resources University). The piston-type wave generator is equipped with an active reflection compensation system (AUKEPC/ARC - DELTARES) and capable of making irregular wave height up to 0.30 m and 3.0s in peak period.

Submerged (platform or island) reefs off the coast of Vietnam are a few hundred meters to several kilometres wide at the flat top level. Note that the morphology of a platform reef considered herein is distinguished from that of a fringing reef in that the reef flat is always submerged and surrounded by the sea, without a shoreline (see Gourlay, 1996a, 1996b). The water depth is often more than 100 m at the reef-foot section and in the range of 5–20 m on the reef flat. This reef-flat submerged depth is substantially larger than that of typical Australian fringing reefs reported in previous studies (e.g. Lowe et al., 2005; Pomeroy et al., 2012; Huang et al., 2012; etc.). The transitional section from the deep water part to the shallow reef flat typically consists of a steep deep foot (slope ~ 1/1-1/2) and a milder flank (slope 1/5-1/15). Because of space constraints it was not possible to scale down the full reef cross-section in the wave flume, only part of submerged reefs which are most relevant to the problem of wave transformation considered was modelled. With further consideration of the test wave conditions the model length scale of 1/40 was eventually selected.

The reef surface in prototype is often very rough with a variety of reef organisms. As a result, wave height attenuation due to bottom friction can be significant in case of small water depths on the reef flat (Lowe et al., 2005; Pomeroy et al., 2012; Huang et al., 2012). Because of relatively large reef-flat water depths and high incoming waves under storm conditions considered in this study (see also Table 1), effects of bottom friction on across-reef wave transformation would be overwhelmingly dominated by depth-induced breaking together with other nonlinear wave processes. On the other hand, albeit effects of bottom friction on wave heights can be considerable, its effects on wave nonlinearities, which eventually influence the wave height distribution, have never been reported in the literature and are difficult to reproduce in small-scale experiments. With the aim to investigate the wave height distribution, on which effects of depth-induced wave breaking are most important, the effect of the reef roughness is therefore disregarded in the present experiments.

Fig. 1 illustrates the experimental layout, in which the model reef is 50 cm high above the flume bottom to assure the generation of incoming deep-water waves. The reef surface was made of smooth and impermeable wooden materials. For the effect of the transitional slope on wave breaking and thus on the wave height distribution, two typical fore-reef slopes of 1/5 and 1/10 are considered, respectively. The flat top width B is 5.0 m (200 m in prototype), sufficiently wide to accommodate both the reef-edge surfzone and the inner reef-flat region (behind the surfzone) for observation of the entire progress of wave transformation over the reef.

Under field conditions, water is able to escape behind a platform reef (without the shoreline) and thus wave setup and wave reflection are minimal (Gourlay, 1996a, 1996b). In flume experiments, however, the landward boundary always exists and therefore these boundary conditions are never fully satisfied. In this study, these laboratory effects were minimized with the introduction of a relative wide basin (12 m) behind the reef and a very gentle riprap slope (slope of 1/6) as a passive wave absorber at the end of the flume.

Capacitance wave gauges are distributed in three regions across the reef, i.e. deep water, reef-edge surfzone and behind the surfzone, in which positions of those on the reef flat can be variable depending on test scenarios so that various across-reef wave conditions can be captured (see Fig. 1 for a standard arrangement of gauges). The sampling rate was set at 50 Hz for all wave gauges.

The experimental program as outlined in matrices of Table 1 consists of 120 test cases, which are combinations of six submerged depths, two fore-reef slopes and ten test waves characterizing various sea states during storms. The test waves were JONSWAP spectra with the peak enhancement factor $\gamma^* = 1.25$ as found most suitable for storm waves at the deep-sea region off the coast of Vietnam. Note that the wave parameters as shown in Table 1 are nominal (steering) at the wave board boundary only, in which the peak wave periods are derived according to two typical storm wave steepness s_{0p} of 0.03 and 0.04, respectively. Amongst these test combinations, test cases with notable super-elevated water levels behind the reef or with largest wave heights in excess of the flume height were excluded. In total, only 108 out of 120 experiments were carried out, each of which lasted approximately 1000 waves to sufficiently cover the main frequency domain of desired wave spectra and allow for stable statistical properties of wave heights. These extensive experiments are considered sufficient to cover wide ranges of variations and combinations of the major independent variables involved (i.e. reef-flat water depth, fore-reef slope, wave height and wave period).

Wave reflection was analyzed with measured records from a three-gauge array at the deep offshore section according to the approach by Zelt and Skjelbreia (1992). To avoid problem of singularities in the determination of wave reflection the spacing of wave gauges was carefully selected and optimized for all test conditions (see WL, 2004). The measured data include individual wave heights, statistical and spectral wave parameters (e.g. $H_{1/3}$, $H_{1/10}$, $H_{1\%}$, $H_{0.1\%}$, H_{rms}, H_{m0}, T_p, $T_{m-1.0}$) at all stations. Typical spectral and statistical wave parameters are defined according to:

$$m_n = \int_{f_L}^{f_U} f^n S(f) df$$
$$H_{m0} = 4\sqrt{m_0} \tag{1}$$
$$T_{m-1,0} = \frac{m_{-1}}{m_0}$$

$$H_{rms} = \sqrt{\frac{1}{N}\sum_{1}^{N} H_i^2}$$
$$H_{1/3} = \frac{1}{\frac{1}{3}N}\sum_{1}^{\frac{1}{3}N} H_i \tag{2}$$

in which, f is the wave frequency, f_L (= 0.025 Hz) and f_U (= 2.5 Hz) are the considered lower and upper frequencies, respectively, $S(f)$ is the

Table 1
Matrix of experimental program.

Reef-flat depth d (m)			Fore-reef slope tanα (-)		Model			Prototype	
Model	Prototype				H_{m0} (m)		T_p (s)	H_{m0} (m)	T_p (s)
0.15	6.0	×	1/5	×	0.09		1.20	3.6	7.6
0.20	8.0		1/10		0.09		1.40	3.6	8.9
0.25	10.0				0.12		1.40	4.8	8.9
0.30	12.0				0.12		1.60	4.8	10.1
0.35	14.0				0.15		1.55	6.0	9.8
0.40	16.0				0.15		1.80	6.0	11.4
					0.17		1.65	6.8	10.4
					0.17		1.90	6.8	12.0
					0.20		1.80	8.0	11.4
					0.20		2.10	8.0	13.3

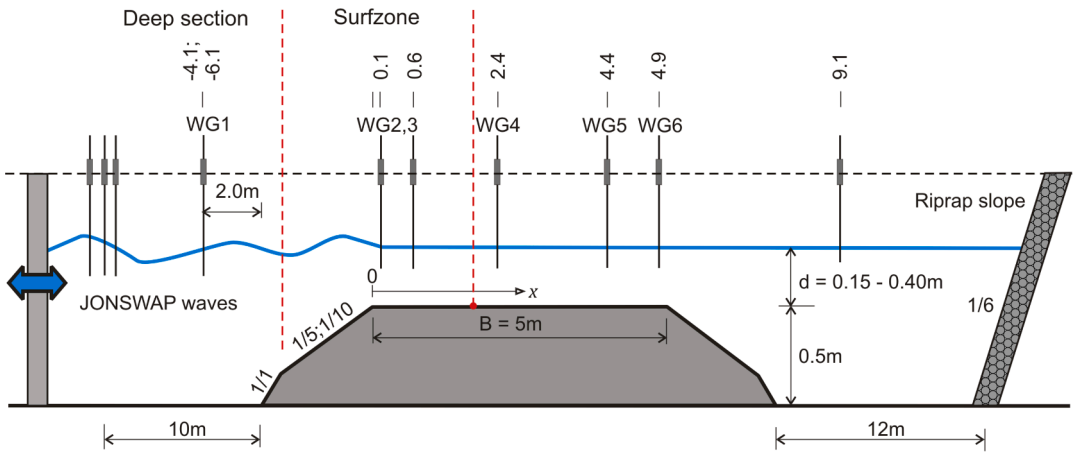

Fig. 1. Layout of experiments of wave transformation across platform reefs.

variance spectral density, m_n is the n-th order spectral moment, $T_{m-1,0}$ is the characteristic spectral period, H_{rms} is the root-mean-square wave height, $H_{1/3}$ is the (statistical) significant wave height, H_{m0} is the (spectral) significant wave height, N is the number of waves in a record, H_i represents the individual wave heights sorted in descending order.

3. Distribution of wave heights on the reef flat

3.1. Influencing parameters and wave height distribution characteristics

In this section, we inspect the measured data of individual wave heights from several systematic test series to gain qualitative understanding of the wave height distribution and influences of reef geometrical and hydraulic parameters.

First, it concerns the effect of the reef-flat shallowness, expressed via the ratio of the incoming deep-water wave to the local water depth over the flat d, on the wave height distribution (see e.g. Hofland et al., 2017 for the definition of beach shallowness). A test series of three different water depths ($d = 0.15$ m, 0.30 m and 0.40 m) under the same typical (moderate) incoming deep-water wave ($H_{m0} = 0.15$ m, $T_p = 1.55$s) and fore-reef slope ($\tan\alpha = 1/10$) are considered. So a smaller depth means a shallower reef flat. Fig. 2 plots the probability exceedance graph of the measured individual wave heights around the reef edge (at WG2) in comparison with the Rayleigh distribution (Longuet-Higgins, 1952), the distribution by Battjes and Groenendijk (2000) and the modified Glukhovskiy (Klopman, 1996). In this figure, the probability of exceedance of a specific wave height is the probability that the wave height shall be reached or exceeded (see also Subsection 3.2). It is shown that the predictive performances of these models are very sensitive to the shallowness of the reef flat. The BG2000 model generally agrees well with the measurements of small waves in the lower part of the distribution, while seriously overestimates those of high waves in the upper part (the tail) of the distribution. The discrepancy with the data markedly extends toward the lower part of the distribution as the shallowness increases corresponding to the decrease in water depth d from 0.40 m in Fig. 2c to 0.15m in Fig. 2a. Particularly, the BG2000 distribution is much steeper than the data trend at the tail, which explains the model overestimation of extreme representative wave heights as noted in Section 1. In contrast to the BG2000 model, the Klopman distribution largely underestimates the measurements, except for very small wave heights. However, in the case of very shallow reef flat the distribution approaches closer to the data points at the tail, i.e. better agreement is found for largest waves (Fig. 2a). The tail of the Klopman distribution and the data trend are generally similar in shape. As expected, the original Rayleigh distribution by Longuet-Higgins (1952) is inappropriate for distribution of wave heights in finite depth.

Second, regarding the influence of the wave height to water depth ratio known as the relative wave energy, Fig. 3 shows the distributions of measured wave heights at various locations across the reef obtained from the same test case ($H_{m0} = 0.15$ m, $T_p = 1.55$s, $d = 0.25$ m and $\tan\alpha = 1/10$). It can be seen that in the surfzone with high relative wave energy (WG2-WG4) the distribution shape (curvature), particularly at the middle part, is most complex and evolves considerably. In the inner reef-flat zone (behind the surfzone) with low relative wave energy (WG5-WG6) the shape becomes rather simple and stable, but seems not revert to a Rayleigh one. At all locations on the reef flat, the tail of the distribution is generally straight and gentle.

Third, for the effect of the fore-reef slope, test cases also under the same incident wave ($H_{m0} = 0.15$ m, $T_p = 1.55$s) and water depth ($d = 0.30$ m), but with two different fore-reef slopes $\tan\alpha = 1/5$ and $1/10$ are considered. Fig. 4 shows the distributions at the reef edge (WG2), inside the surfzone (WG3) and behind the surfzone (WG5), respectively. The fore-reef slope appears to have significant effects on the distribution within the reef-edge surfzone only (Fig. 4a and b). Under the same incoming deep-water waves, a steeper slope results in a greater fore-reef depth and thus the incoming waves at the reef edge are higher (Fig. 4a). However, this increase is not of the same proportionality for all wave heights, especially the lowest waves are almost not affected. Moving further inside the surfzone the largest waves start to break due to depth-limited conditions. As a result, the slope effect is seen to exhibit in the intermediate wave heights only (see Fig. 4b). Because most high waves break within the surf zone, wave heights behind the surfzone are mainly related to the local water depth, blurring out the fore-reef slope effect as seen in Fig. 4c.

Overall, it is apparent that to better describe the wave height distribution its three distinct parts as noted above (i.e. lower, intermediate and upper) should be realized.

3.2. Formulations of a new composite Weibull distribution

The above analysis reveals some important characteristics of the distribution of wave heights on the reef flat, which are hints for the development of a new model. In terms of complexity, one would distinguish between the distribution for locations inside the surfzone and that behind the surfzone. In the surfzone the distribution is more complex than that can be described by a single- or even a two-Weibull distribution (i.e. a combination of two Weibull distributions can be used at the expense of sacrificing the overall agreement). It is therefore suggested that a composite distribution consisting of three distinct segments for small, intermediate and largest wave heights should be used instead. Smallest waves below a certain limit are a little affected by the shallow water depth and thus still fit with a Rayleigh distribution. The tail with largest waves (breaking and near-breaking waves) shows a simple trend of gently sloping line (i.e. small curvature), implying that a

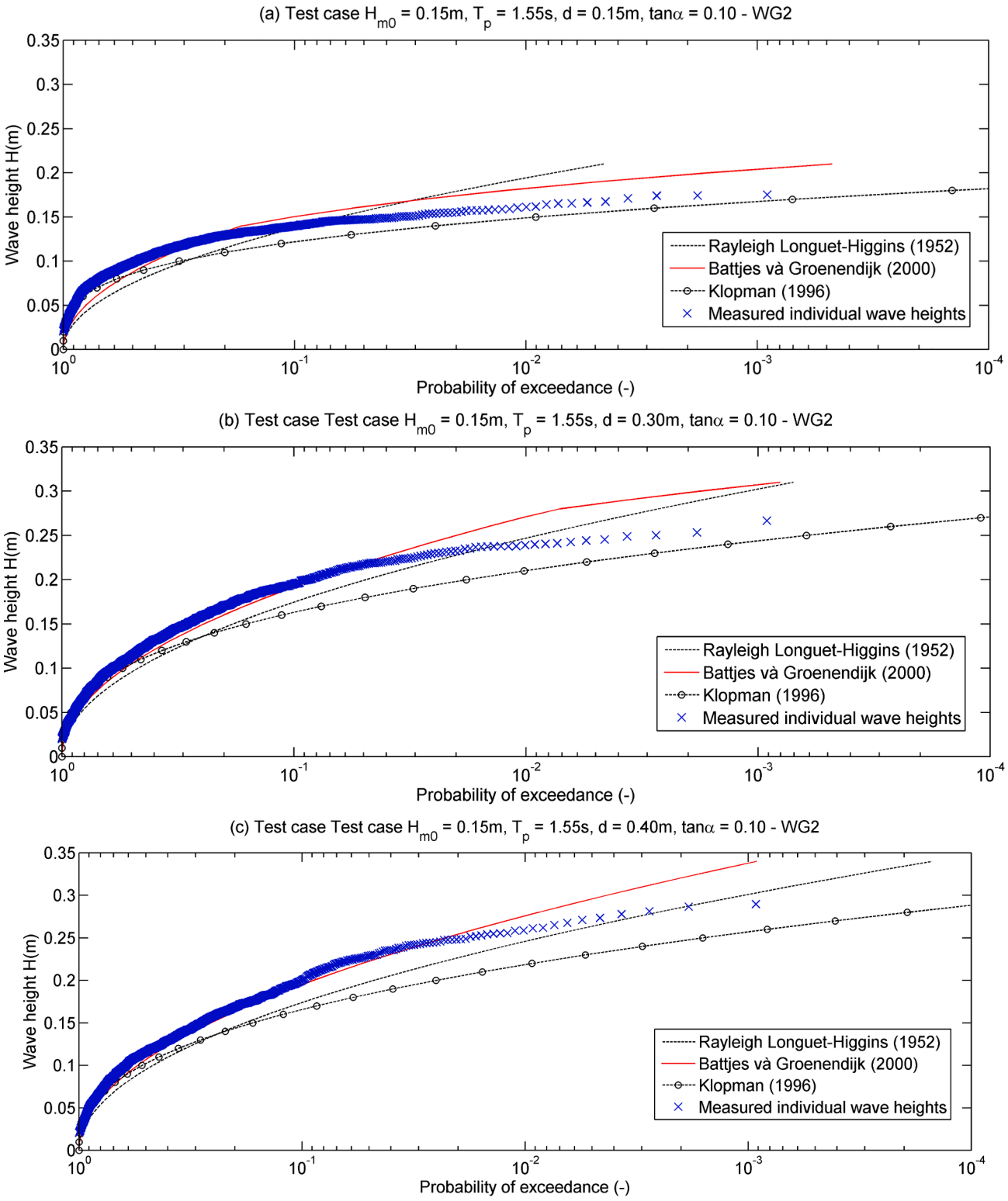

Fig. 2. Wave height distribution at the reef edge compared with existing distributions, effects of water depth d on the reef flat (under the same incoming wave $H_{m0} = 0.15$ m, $T_p = 1.55$s and the same fore-reef slope tanα = 1/10): (a) $d = 0.15$ m (b) $d = 0.30$ m (c) $d = 0.40$ m

Weibull with a large exponent for the upper part would be appropriate. Whereas, because of depth-induced breaking and nonlinear effects the mid part with intermediate wave heights (shoaling waves and broken waves) evolves considerably, which contradicts with that in the case of shallow beaches (see Battjes and Groenendijk, 2000). This evolving part eventually affects the overall model predictive performances via its connections to lower and upper ones. Behind the surfzone the distribution collapses to a simpler one which can well be described with a Rayleigh-Weibull distribution.

The concept of three-Weibull distribution (henceforth referred to as 3WD) is illustrated in Fig. 5. Following the same approach by Battjes and Groenendijk (2000), the general expressions of the distribution in case all three Weibull segments exist are as follows:

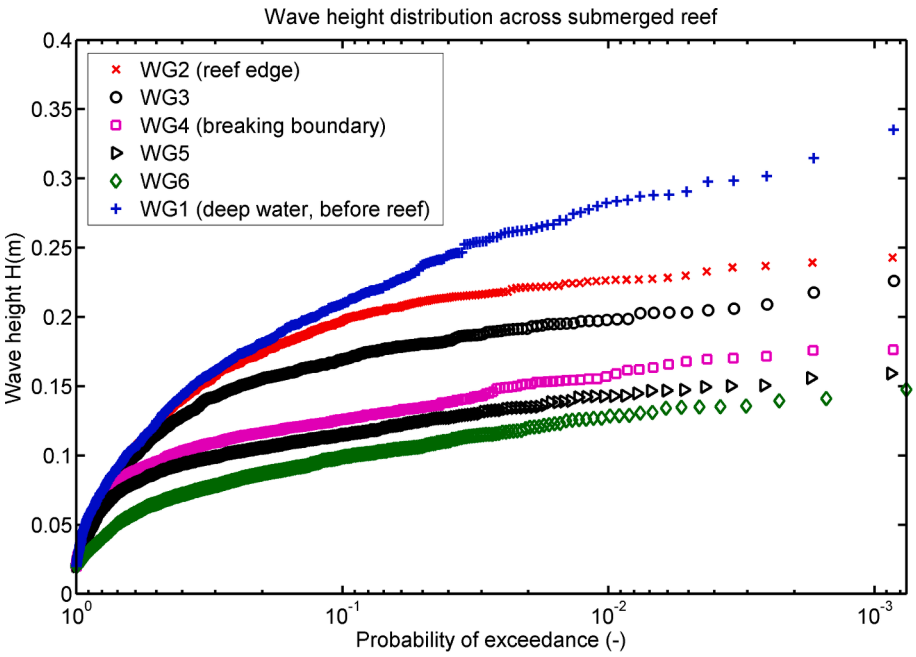

Fig. 3. Distributions of wave heights across the reef flat, test case: $H_{m0} = 0.15$ m, $T_p = 1.55$s, $d = 0.25$ m and $\tan\alpha = 1/10$.

$$\Pr\{\underline{H} < H\} = \begin{cases} F_0(H) = 1 - \exp\left[-\left(\dfrac{H}{H_*}\right)^2\right] & H \le H_{tr,0} = 0.35d \\ F_1(H) = 1 - \exp\left[-\left(\dfrac{H}{H_1}\right)^{k_1}\right] & H_{tr,0} \le H \le H_{tr} \\ F_2(H) = 1 - \exp\left[-\left(\dfrac{H}{H_2}\right)^{k_2}\right] & H \ge H_{tr}; H_{tr} \le H_{\max} \end{cases} \tag{3}$$

in which H^*, H_1 and H_2 are scale wave heights of the corresponding Weibull functions, exponents k_1 and k_2 are shape factors, d is the water depth on the reef flat, $\Pr\{\underline{H} < H\}$ is the probability of non-exceedance of wave height (or $\Pr\{\underline{H} \ge H\}$is the probability of exceedance).

Note that the 3WD in general has two distinct transitional wave heights $H_{tr,0}$ and H_{tr}. As argued above the first (lower) transitional height $H_{tr,0}$ is treated like a threshold, below which waves are negligibly affected by shallow water and thus a Rayleigh distribution is valid. In this sense, $H_{tr,0}$ must be a small fraction of the water depth d only. Through fitting a Rayleigh distribution for the lower part we found that $H_{tr,0} = 0.35d$ gives the best overall agreement with the experimental data. As noticed earlier the second (upper) transitional height H_{tr} would vary with not only on the bottom topography but also with wave breaking intensity or the reef-flat shallowness.

In case the 3WD shrinks to a two-Weibull distribution, the third expression in Eq. (3) is omitted and only the first transitional wave height $H_{tr,0}$ remains, similar to the BG2000 model. The criterion for this is discussed in Section 3.3.4.

The 3WD model as a whole must satisfy the continuity conditions at the two transitional wave heights and the expression for the root-mean square (RMS) wave height H_{rms}, respectively:

$$F_0(H_{tr,0}) = F_1(H_{tr,0}) \tag{4}$$

$$F_1(H_{tr}) = F_2(H_{tr}) \tag{5}$$

$$H_{mrs} = \sqrt{\int_0^{H_{tr,0}} H^2 f_0(H)dH + \int_{H_{tr,0}}^{H_{tr}} H^2 f_1(H)dH + \int_{H_{tr}}^{\infty} H^2 f_2(H)dH} \tag{6}$$

After some algebraic manipulations Eqs. (4)–(6) can respectively be rewritten in dimensionless forms as follows (see e.g. Groenendijk and van Gent, 1998):

$$\left(\frac{\widehat{H}_{tr,0}}{\widehat{H}_*}\right)^2 = \left(\frac{\widehat{H}_{tr,0}}{\widehat{H}_1}\right)^{k_1} \tag{7}$$

$$\left(\frac{\widehat{H}_{tr}}{\widehat{H}_1}\right)^{k_1} = \left(\frac{\widehat{H}_{tr}}{\widehat{H}_2}\right)^{k_2} \tag{8}$$

$$1 = \sqrt{\widehat{H}_*^2 \gamma\left[\left(\frac{\widehat{H}_{tr,0}}{\widehat{H}_*}\right)^2,\ 2\right] + \widehat{H}_1^2\left(\gamma\left[\left(\frac{\widehat{H}_{tr}}{\widehat{H}_1}\right)^{k_1}, \frac{2}{k_1}+1\right] - \gamma\left[\left(\frac{\widehat{H}_{tr,0}}{\widehat{H}_1}\right)^{k_1}, \frac{2}{k_1}+1\right]\right) + \widehat{H}_2^2 \Gamma\left[\left(\frac{\widehat{H}_{tr}}{\widehat{H}_2}\right)^{k_2}, \frac{2}{k_2}+1\right]} \tag{9}$$

where $\widehat{H}_x$ is a normalized height of H_x with respective to H_{rms} ($\widehat{H}_x = H_x/H_{rms}$), Γ and γ are upper and lower incomplete gamma functions, respectively.

When only first two Weibull distributions exist, Eq. (9) becomes:

$$1 = \sqrt{\widehat{H}_*^2 \gamma\left[\left(\frac{\widehat{H}_{tr,0}}{\widehat{H}_*}\right)^2,\ 2\right] + \widehat{H}_1^2 \Gamma\left[\left(\frac{\widehat{H}_{tr,0}}{\widehat{H}_1}\right)^{k_1}, \frac{2}{k_1}+1\right]} \tag{10}$$

For the determination of the 3WD a system of three equations Eqs.

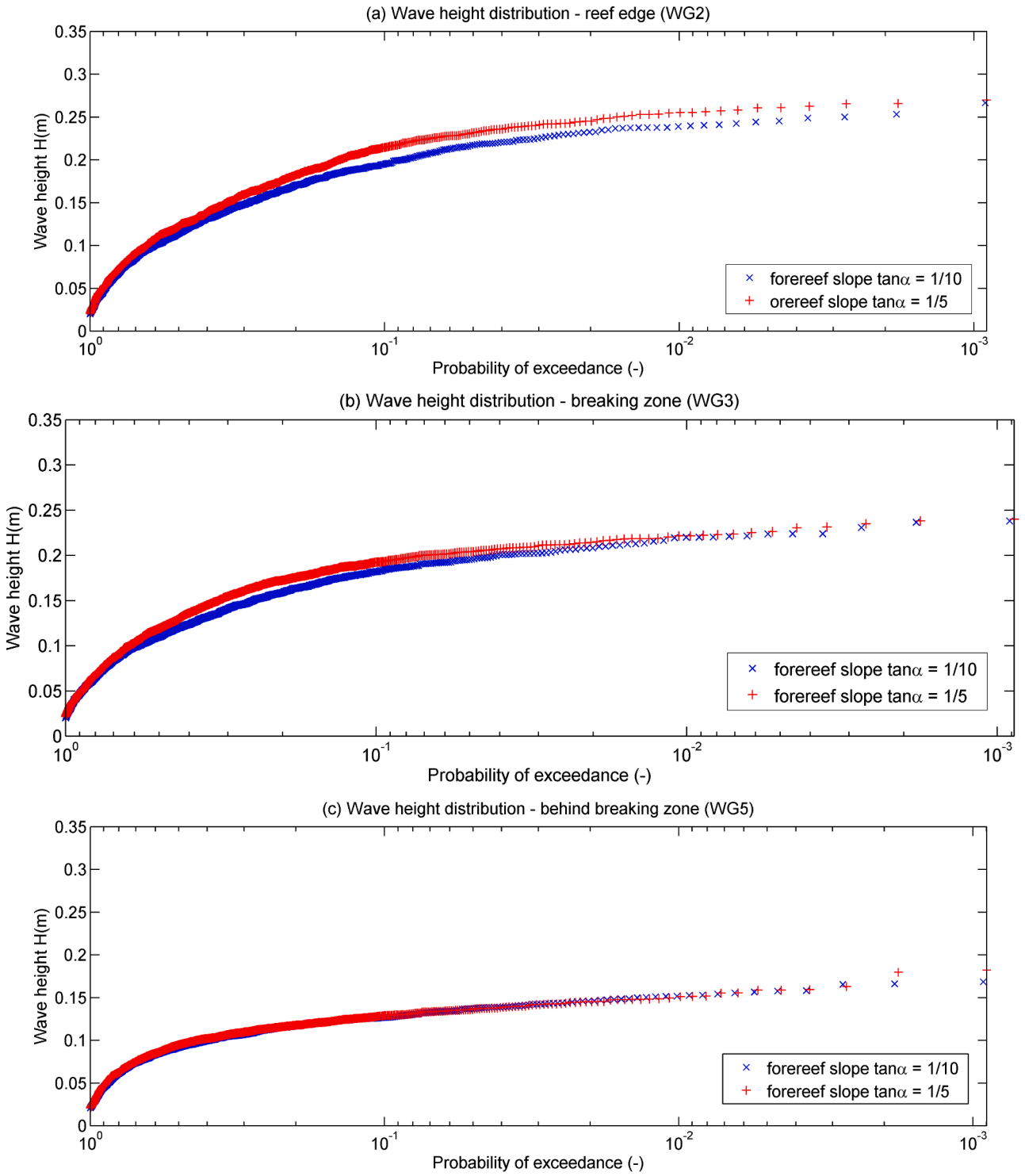

Fig. 4. Effects of fore-reef slope under the same incident wave $H_{m0} = 0.15$ m, $T_p = 1.55$s: (a) at the reef edge (b) inside the surfzone (c) behind the surfzone.

(7)–(9) with three unknowns H^*, H_1 and H_2 needs to be solved numerically. The model parameters H_{tr}, k_1 and k_2 ($H_{tr,0}$ is already determined, $H_{tr,0} = 0.35d$) are known because, as shown in the following section, they are related to the input parameters such as bottom slope, water depth and wave spectral parameters.

3.3. Parameterization of model parameters

The existing point models incorporating wave breaking effects discussed so far assume a slow wave evolution so that the model parameters can well be related to the local conditions only (e.g. the bottom slope, water depth and wave spectral energy at a considered location), regardless of the wave propagation history from deep-water. As shown in Battjes and Groenendijk (2000) this assumption is generally valid for cases of relatively simple bottom topography such as gently-sloping beaches. Herein, as discussed earlier (Fig. 4a and b) the influence of the fore-reef slope, which somewhat reflects the wave propagation history, clearly exhibits in the wave height distributions in the surf zone. This means that in addition to the local wave spectral energy and the local water depth, the fore-reef slope rather than the local bed slope of

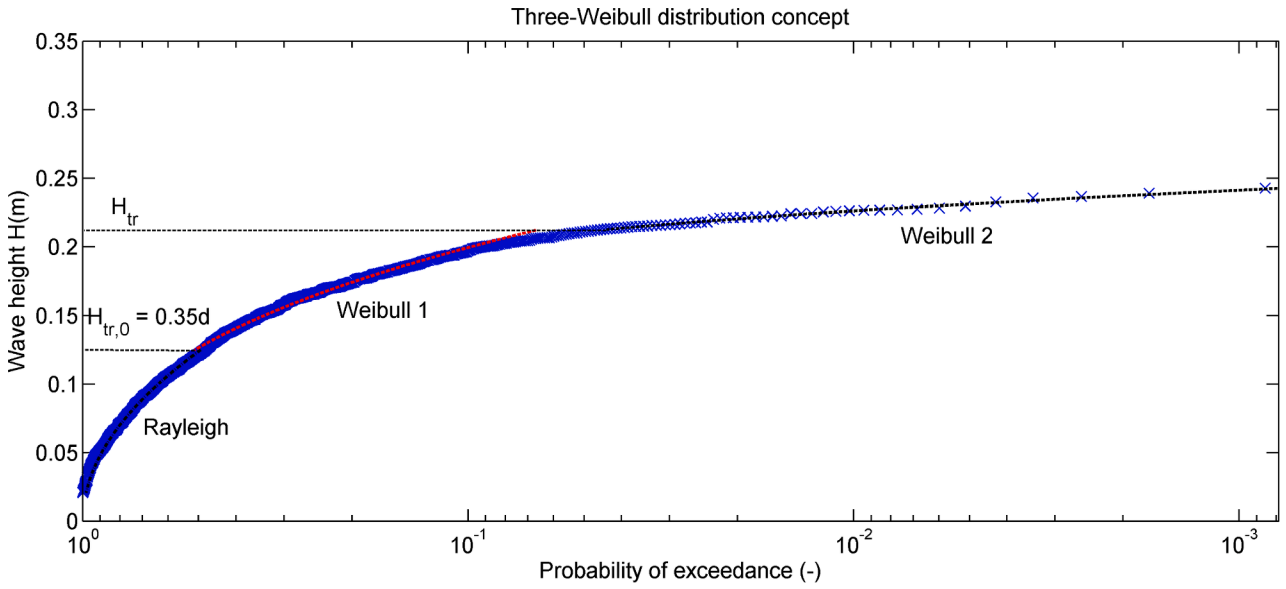

Fig. 5. Concept of three-Weibull distribution model (3WD).

the reef flat should be used for the model parameterization, at least for locations inside the reef-edge surfzone. Nevertheless, this slope dependency seems relatively weak as it in part implicitly reflects through the fore-reef water depth in scaling wave heights on the reef flat. Behind the surfzone, the fore-reef slope influence becomes negligibly small and thus the local bed slope should be used instead.

In the following we shall relate the three model parameters, i.e. H_{tr}, k_1 and k_2, to the external input parameters. The values of these are first experimentally determined though least-squares fitting the 3WD (Fig. 5) with all individual wave heights from each of 540 measured records from five stations across the reef flat.

3.3.1. *Upper transitional wave height H_{tr}*

For the composite type of distributions, proper transitions are very essential for the model reliability. As shown earlier, the BG2000 model consistently over-estimates the transitional wave height, which in combination with a steep Weibull tail aggravates the model over-prediction of highest wave heights. This is in part due to the fact that the transitional wave height H_{tr} in the BG2000 model was formulated with the datasets of a few representative wave heights only (not all individual wave heights).

By definition, the upper transitional wave height H_{tr} of the 3WD lies between the mid part of broken and shoaling waves and the upper one of breaking and near-breaking waves. When H_{tr} becomes too large, i.e. exceeding the maximum wave height, the third Weibull part does not exist.

As hinted at above, the wave height distribution depends on the shallowness of the reef flat. In this study, we propose a new parameter χ:

$$\chi = \frac{\cos\alpha}{\sqrt{d/L_{0m}}} \tag{11}$$

in which, α is the fore-reef slope for locations inside the surfzone, and $\alpha = 0$ ($\cos\alpha = 1$) behind the surfzone, L_{0m} ($= g/(2\pi)T_{m-1,0}^2$) is the deep-water wave length based on the local characteristic wave period $T_{m-1,0}$.

The parameter χ is a measure of the local shallowness on the reef flat. A larger value of χ means a relatively shallower condition and vice versa. The use of $\cos\alpha$ in Eq. (11) is due to the weak dependency of the fore-reef slope noticed earlier. Note also that behind the surfzone where the relative wave intensity is sufficiently small (see Sections 3.3.3 and 3.3.4), the slope effect becomes negligible and thus $\cos\alpha = 1$ can be used in Eq. (11).

Similar to the situation on a shallow foreshore, because of severe wave breaking wave spectra across the shallow reef flat tend to flatten out or exhibit multiple peaks. Moreover, compared to open gentle beaches, IG waves are enhanced on steep reefs and can account for a significant proportion in the total wave energy on the reef flat (see also Section 5). In such a case, the use of a mean spectral period having emphasis on longer-period waves in shallow water like $T_{m-1,0}$ rather than the peak spectral period is therefore preferable in describing the wave-structure interaction (see e.g. Van Gent, 2001; Tuan et al., 2016). Moreover, the local wave period $T_{m-1,0}$ is indeed related to the beach shallowness represented by the ratio of deep-water wave height to local water depth (see e.g. Hofland et al., 2017). In this study we also advocate the use of $T_{m-1,0}$ as the input wave period to the model. This characteristic period $T_{m-1,0}$ is a common output from wave models and can also be estimated using empirical formulas (see EurOtop, 2018).

The relative transitional wave height $H_{tr}/\sqrt{m_0}$ is plotted against χ for various locations in Fig. 6. It appears from comparison between the number of data points associated with locations within the surfzone (WG2-WG4) and those behind the surfzone (WG5, WG6) that the 3WD always exists with complete three parts within the surfzone and often collapses to contain only the first two Weibull ones behind the surfzone (a data point is missing once H_{tr} is undetermined or the third Weibull does not exist).

The following formulation of the transitional wave height H_{tr} is found by a least-square fit of all the experimental data shown in Fig. 6 with satisfactory agreement ($R^2 = 0.70$).

$$\frac{H_{tr}}{\sqrt{m_0}} = \frac{3.96}{\tanh(0.30\cdot\chi)} \tag{12a}$$

$$H_{tr} \approx \frac{H_{m0}}{\tanh(0.30\cdot\chi)} \tag{12b}$$

where 3.96 (3.82, 4.10) and 0.30 (0.28, 0.32) are regression coefficients and their corresponding 95% confident bands.

Note from Fig. 6 and Eq. (12) that the ratio $H_{tr}/\sqrt{m_0}$ approaches the lower limit of 3.96 or $H_{tr} = 3.96\sqrt{m_0} \approx H_{m0}$ when χ is sufficiently large (i.e. in very shallow water, $\chi \geq 7.0 \rightarrow \tanh(0.3\cdot\chi) \rightarrow 1.0$). In relatively deeper locations, the transitional height H_{tr} rapidly increases as χ declines. When χ is too small H_{tr} becomes in excess of the maximum wave height, omitting the third Weibull part (see also Section 3.3.4).

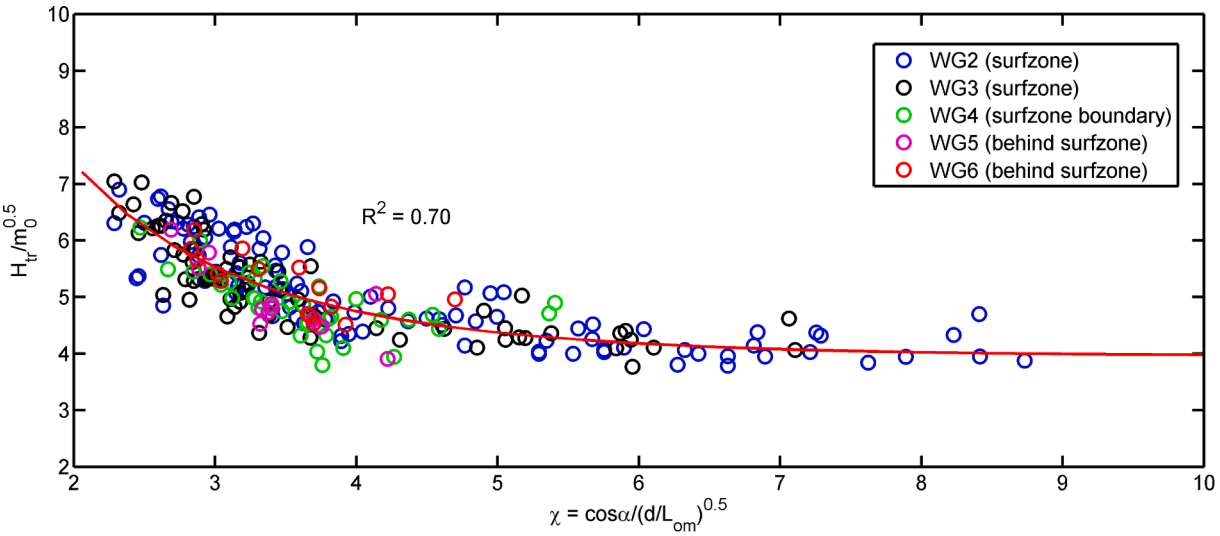

Fig. 6. Relation.$H_{tr}/\sqrt{m_0}\sim\chi$

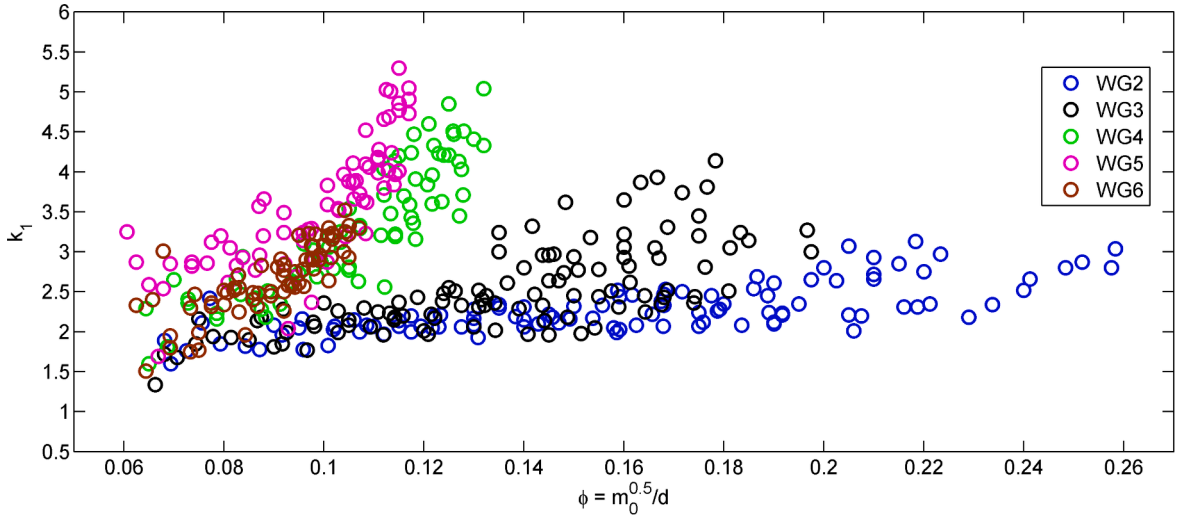

Fig. 7. Variation of k_1 with local relative wave intensity.$\phi = \sqrt{m_0}/d$

3.3.2. *Exponents k_1 and k_2*

It follows from the analysis in Section 3.1 that the exponent k_1 (curvature of the middle part) varies considerably with the local parameters, while the variation of k_2 is rather mild. Therefore, the use of a fixed exponent for the Weibull distribution like in the BG2000 model for a variety of wave conditions seems inappropriate (see also e.g. Christou et al., 2011; Caires and van Gent, 2012). In the following we explore the effect of the local conditions on the determination of these exponents in terms of both the local relative wave intensity ϕ and the local shallowness χ.

Fig. 7 plots the variation of k_1 with the relative wave intensity ϕ ($=\sqrt{m_0}/d$). Similar to the finding by Battjes and Groenendijk (2000) large scattering in k_1 values is observed for locations with small relative wave density, particularly behind the surfzone (WG4-WG6). However, if the effect of the local shallowness χ is also accounted for in formulating k_1, expressed as k_1/χ, a reasonably good agreement in the data representation can be obtained (see Fig. 8). Accordingly, the expression for k_1 can be discriminated into two cases of low and high ϕ-values, respectively:

$$\begin{aligned} \frac{k_1}{\chi} &= 0.86 && \phi < 0.10 \\ \frac{k_1}{\chi} &= 0.86 - 4.13(\phi - 0.10) && 0.10 \le \phi < 0.31 \end{aligned} \tag{13}$$

Note that the boundary at $\phi = 0.10$ between the low and high relative wave intensity regions somewhat coincides with that noted in Battjes and Groenendijk (2000). It is emphasized that, as shown in the following, this boundary is consistently found in formulating all other model parameters and turns out to be essential for the parameterization of the 3WD.

The k_2-data plotted against each of ϕ and χ are shown in Fig. 9a and b, respectively. Again, large scattering is seen for the region of low ϕ-values ($\phi < 0.10$, mostly broken waves behind the surfzone) or with small χ-values ($\chi \le 3.5$). In the region of high ϕ-values ($\phi \ge 0.10$) or relatively shallow water ($\chi > 3.5$) the scattering is considerably reduced and k_2 tends to vary about a constant mean value (≈ 4.70). Intuitively, the number of k_2-data points are much less than those of k_1 due to the collapse of the 3WD in the area of low relative wave intensity as noticed earlier. A closer inspection of the data also reveals that cases without k_2

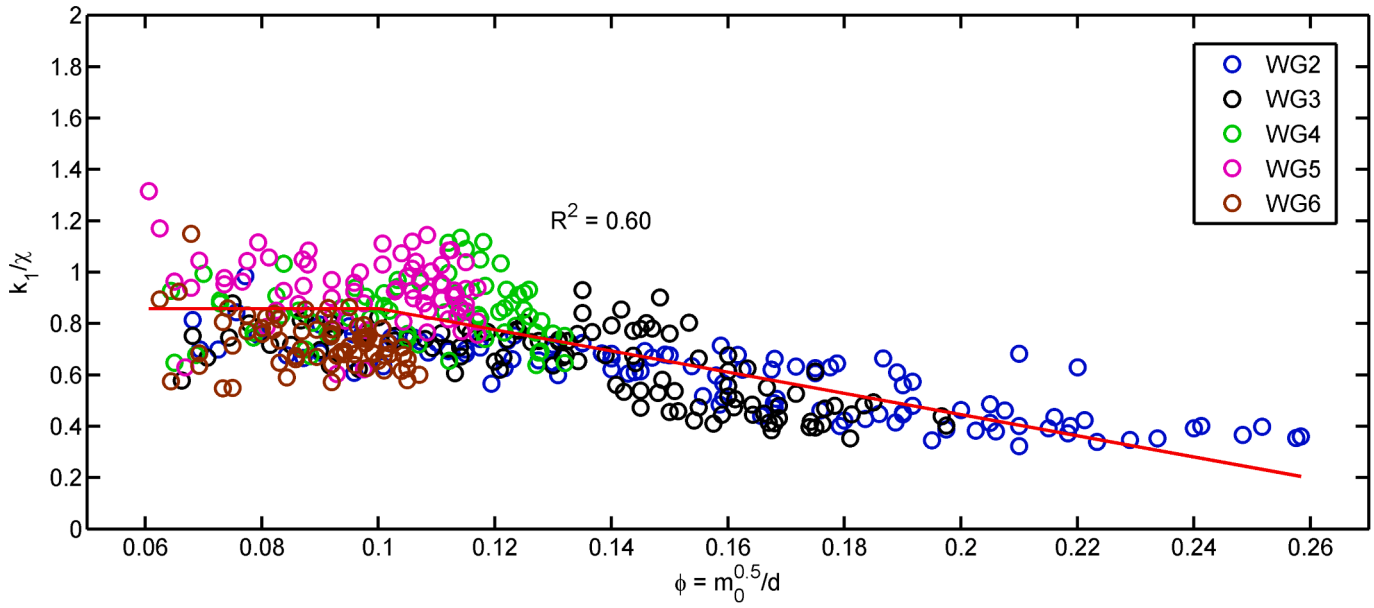

Fig. 8. Variation of k_1/χ with local relative wave intensity $\phi = \sqrt{m_0}/d$.

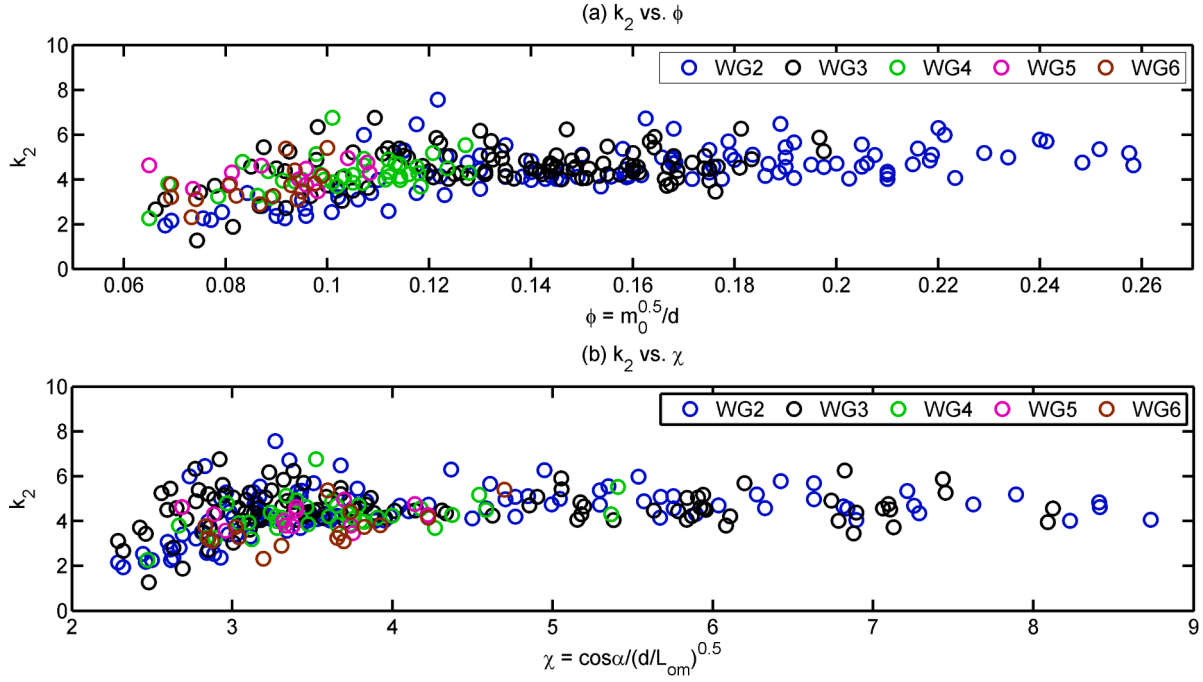

Fig. 9. Variation of k_2 with local conditions: (a) k_2 vs. ϕ (b) k_2 vs. χ

all fall within the range of low ϕ-values. Out of all the cases considered in this range (corresponding with number of k_1-data points in Fig. 7) a vast number of cases (151 out of 253 cases) are with k_2 undetermined. In the range of low ϕ-values, k_2-values, though determined, are very close to those of k_1, implying that the third Weibull part might not be necessary. These arguments on the exponent k_2 suggest that the two-Weibull distribution is most appropriate (i.e. k_2 is absent) when $\phi < 0.10$. The exponent k_2 is thus determined as a constant for locations with high ϕ-values only:

$$k_2 = 4.70 \quad \phi \geq 0.10 \tag{14}$$

3.3.3. *Root-mean-square wave height H_{rms}*

To fully determine the 3WD, apart from the model parameters addressed so far, the RMS wave height H_{rms} needs to be quantified in connection with the local spectral wave energy m_0. For this, the ratio $H_{rms}/\sqrt{m_0}$ plots against the relative wave intensity ϕ in Fig. 10. It is well-known that due to wave nonlinearities in shallow water this ratio becomes higher than that of Rayleigh waves in deep water (see also discussions on effects of IG waves in Section 5). This was also reported in Battjes and Groenendijk (2000) though a linearly proportional relation of $H_{rms}/\sqrt{m_0}$ with ϕ, starting from the lower boundary $H_{rms}/\sqrt{m_0} = 2.69$, stipulated by finite bandwidth waves in deep water. Herein, the increase of $H_{rms}/\sqrt{m_0}$ in shallow water on the reef flat is reaffirmed but a somewhat different trend is observed. For low ϕ-values ($\phi < 0.10$), the ratio $H_{rms}/\sqrt{m_0}$ varies about the same lower boundary of 2.69. For high-ϕ values ($\phi \geq 0.10$) it gradually increases with the

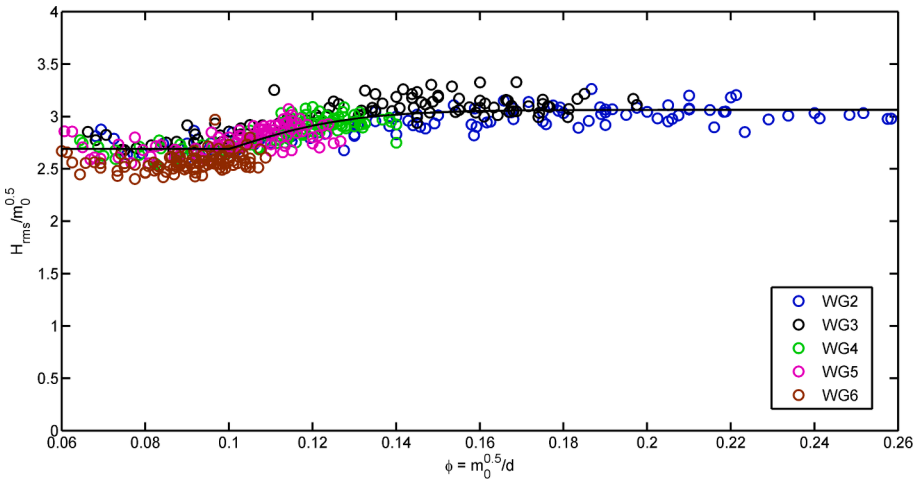

Fig. 10. Variation of H_{rms} with local relative wave intensity ϕ

increase of ϕ and approaches an upper limit of approximately 3.10.

A least-square fit of the experimental data results in the following formulations of H_{rms} for low- and high-ϕ regions, respectively:

$$\frac{H_{rms}}{\sqrt{m_0}} = 2.69 \quad \phi < 0.10$$
$$\frac{H_{rms}}{\sqrt{m_0}} = 2.69 + 0.37\tanh[34.2(\phi - 0.1)] \quad \phi \geq 0.10 \tag{15}$$

3.3.4. Collapse of the 3WD and the practical upper limit of wave heights

As shown in previous sections the model parameters k_1, k_2 and H_{mrs} all switch their behaviours at almost the same critical value of the relative wave intensity ϕ. Particularly, the exponent k_2 is undetermined at large for $\phi < 0.10$. These observations lend support to the assumption, important for the model reliability, that the 3WD collapses from a full three-Weibull distribution to a two-Weibull one when ϕ becomes sufficiently small. Overall, the critical value of ϕ between the two regions of low and high ϕ-values herein has been set at $\phi_{cr} = 0.10$ as evidenced by the experimental data. Locations of low ϕ-values on the reef flat are often well behind the surfzone, where only broken and small non-breaking waves remain.

It is possible to theoretically verify the chosen critical value ϕ_{cr}. Since the third Weibull of the 3WD co-exists with the upper transitional wave height H_{tr}, the critical ϕ value can be derived in accordance with the criterion for the existence of H_{tr}. By definition, the third Weibull exists only if the largest wave height is not exceeded by H_{tr}, i.e. $H_{tr} < H_{\max}$ (see also Fig. 5). From Eq. (11) together with Eq. (12b) this criterion can be worked out as follows:

$$\chi > \chi^* = 3.33\,\text{atanh}\left(\frac{1}{\beta}\right) \tag{16}$$

or in terms of ϕ:

$$\phi = \frac{\sqrt{m_0}}{d} > \frac{\chi_*^2}{4\cos\alpha^2} s_{0m} \tag{17}$$

in which, $\beta = H_{\max}/H_{m0}$, χ^* is a critical value of χ, s_{0m} ($= \frac{2\pi H_{m0}}{gT_{m-1,0}^2}$) is the fictitious wave steepness.

In deep water, the ratio $H_{\max}/H_{m0}$ is approximately equal to 1.80 based on the Rayleigh distribution by Longuet-Higgins (1952). In shallow water, this ratio declines with the increase of wave breaking intensity. In this study, the relation between β and the shallowness factor χ obtained from the measurements on the reef flat is presented in Fig. 11, showing that from very shallow to relatively deeper water conditions the value of β, on average, varies from 1.50 to 2.0. Typically, $\beta = 1.50$ is found representative for a wide range of shallow conditions ($\chi > 3.0$) and is thus used for consideration herein. The experimental data also show that s_{0m} is in the range between 0.030 and 0.055 at high ϕ-values. With $\beta = 1.50$ ($\chi^* = 2.70$ from Eq. (14)) and the value range of s_{0m} substituted, the criterion for the existence of the third Weibull of the 3WD can eventually be deduced from Eq. (17): $\phi > 0.06$–0.10. This asserts that the critical value $\phi_{cr} = 0.10$ is in fact appropriate.

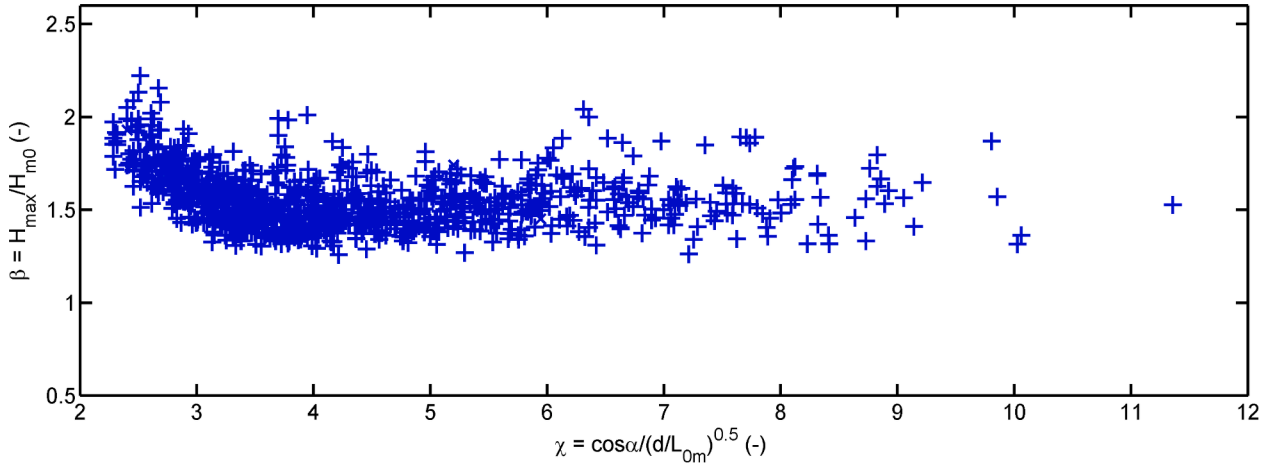

Fig. 11. Variation of $H_{\max}/H_{m0}$ with local shallowness χ

As addressed in Section 1, to improve the model predictive performance on largest wave heights the tail of the distribution should realistically be intercepted by an upper limit for wave heights in shallow water. This upper limit is implicit in the 3WD but can be evaluated through assessing the maximum wave height predicted by the model. Largest wave heights in case the 3WD collapses are generally smaller than those when all three Weibull parts exist. It is therefore sufficient to consider the maximum wave height in the latter case. It follows from the third Weibull in Eq. (3):

$$\frac{H_{\max}}{H_2} = [\ln(N)]^{1/k2} < 1.54 \tag{18}$$

where $H_{\max}$ is the maximum wave height in N considered waves. For the evaluation of $H_{\max}$, N is often taken as 1000 waves under laboratory conditions ($H_{\max} = H_{0.1\%}$), though sometime can be up to several thousands of waves. However, owing to the large exponent k_2 the ratio $H_{\max}/H_2$ is relatively insensitive to N (i.e. $H_{\max}/H_2 = 1.51$–1.54 with $N = 1000$–2000). Herein, for considering the practical upper limit $N = 2000$ is taken on the conservative side, giving the value of 1.54 on the right hand side of Eq. (18).

It appears from the relation ($H_2/H_{m0} \sim \phi$) shown in Fig. 12 that the ratio H_2/H_{m0} is approximately unity with a maximum deviation of about 0.20 at $\phi < 0.13$, i.e. $H_2/H_{m0} = 1.0 \pm 0.2$. Hence, the practical upper limit of wave heights H_{UL} expressed in terms of H_{m0} can be derived from Eq. (18):

$$H_{\max} \le H_{UL} = (1.3 - 1.9)H_{m0} \tag{19}$$

The upper limit of wave heights H_{UL} specified in Eq. (19) lies within the range of maximum wave height in shallow water (see also Fig. 11), whereby largest wave heights predicted by the 3WD are realistically intercepted.

3.3.5. Summary of calculation steps

Given all necessary local inputs, i.e. m_0, $T_{m-1,0}$, d and $\tan\alpha$, the following steps are taken for establishing the 3WD and then determining characteristic wave heights at a considered location on the reef flat.

(1) Calculation of the relative wave intensity ϕ and checking the collapse of the 3WD:
   * If $\phi < 0.10$, only two Weibull parts exist, continue with step (3).
   * If $\phi \ge 0.10$, all three Weibull parts exists, continue with step (2);

(2) Calculation of transitional wave heights $H_{tr,0}$ and H_{tr}:
   * The lower transitional wave height $H_{tr,0} = 0.35\,d$
   * The upper transitional wave height H_{tr}:
     - The shallowness parameter χ is calculated according to Eq. (11);
     - The upper transitional wave height H_{tr} is determined according to Eq. (12).

(3) Determination of the exponents k_1, k_2
   * The exponent k_1 is calculated according to Eq. (13);
   * The exponent k_2 is determined only if $\phi \ge 0.10$, $k_2 = 4.70$ (Eq. (14)).

(4) Establishment of the 3WD

The RMS wave height H_{rms} is calculated according to Eq. (15). It then follows by the determination of scale wave heights H^*, H_1 and H_2.

* If $\phi < 0.10$, Eqs. (7) and (10) are numerically solved for H^* and H_1.
* If $\phi \ge 0.10$, Eqs. (7)–(9) are numerically solved for H^*, H_1 and H_2.

The 3WD is fully established through the system of equation (3), whereby any arbitrary characteristic wave heights such as $H_{1/3}$, $H_{1/10}$, $H_{1\%}$, $H_{0.1\%}$, etc. can be calculated.

4. Model comparison and validation

4.1. Model comparison with data of characteristic wave heights

The model parameters of the 3WD have been formulated based on overall agreements with all individual wave heights from the measured wave records. Still, it is necessary to examine the model predictive performance on most common characteristic wave heights. For this, comparisons of wave heights $H_{1/3}$, $H_{1/10}$, $H_{1\%}$ and $H_{0.1\%}$ between the data from all 540 measured records and those predicted by the 3WD and the BG2000 model are shown in Figs. 13 and 14, respectively. As hinted at in Subsection 3.1 on the bed slope effect (see also Fig. 4), the local bed slope as input to the BG2000 model is specified as the fore-reef slope for locations within the reef-edge surfzone and as 1/250 for those behind this boundary (BG2000 is not valid for flat bottoms). The goodness of the model predictions is evaluated through the relative mean-square error ε:

$$\varepsilon = \sqrt{\frac{\sum_{i=1}^{N_p}\left(1 - \frac{H_{model,\,i}}{H_{lab,\,i}}\right)^2}{N_p}} \tag{20}$$

in which, H_{model} and H_{lab} denote wave heights predicted by the model

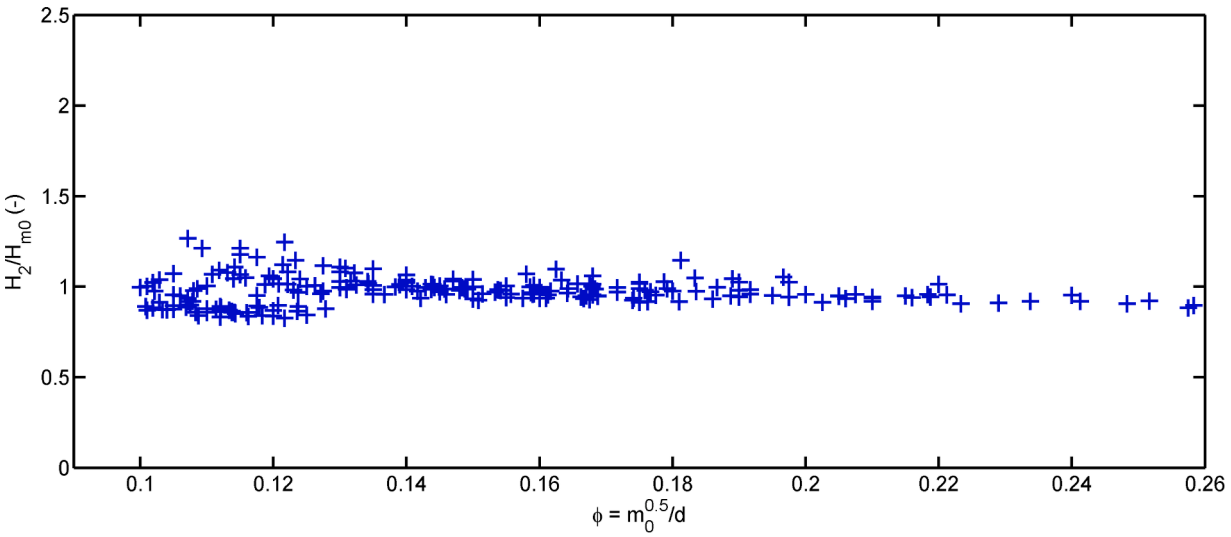

Fig. 12. Variation of H_2/H_{m0} with ϕ

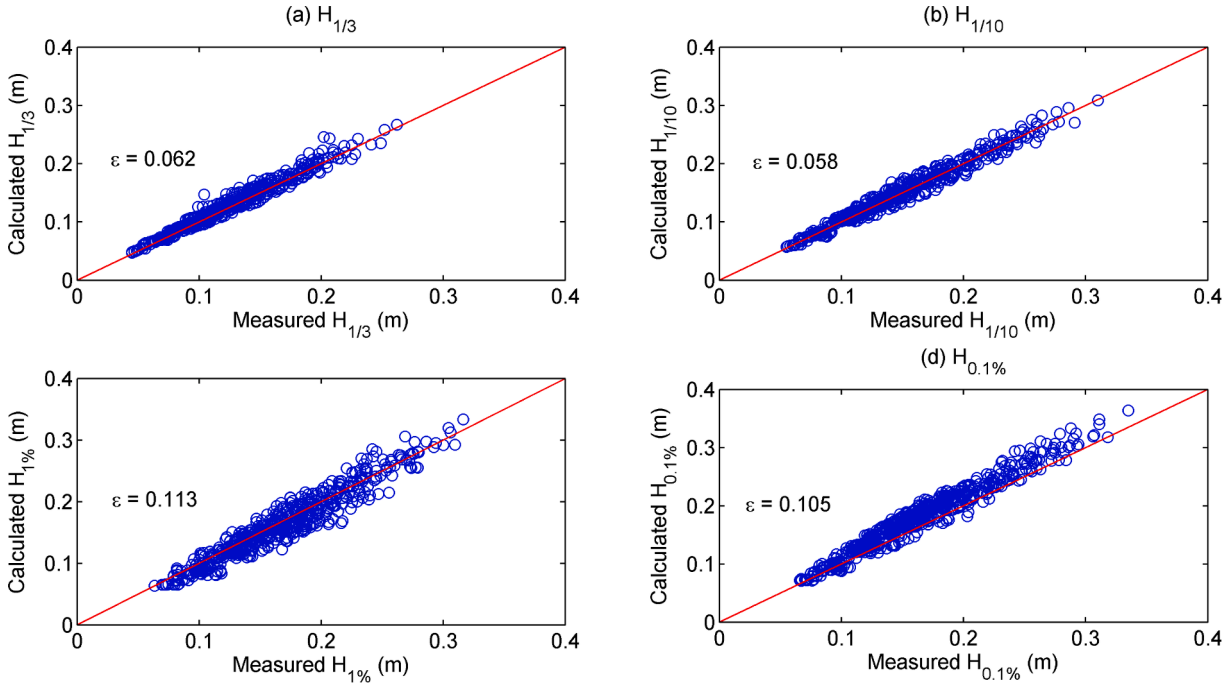

Fig. 13. Characteristic wave heights predicted by the 3WD (present study) compared with measurements: (a) $H_{1/3}$ (b) $H_{1/10}$ (c) $H_{1\%}$ (d) $H_{0.1\%}$.

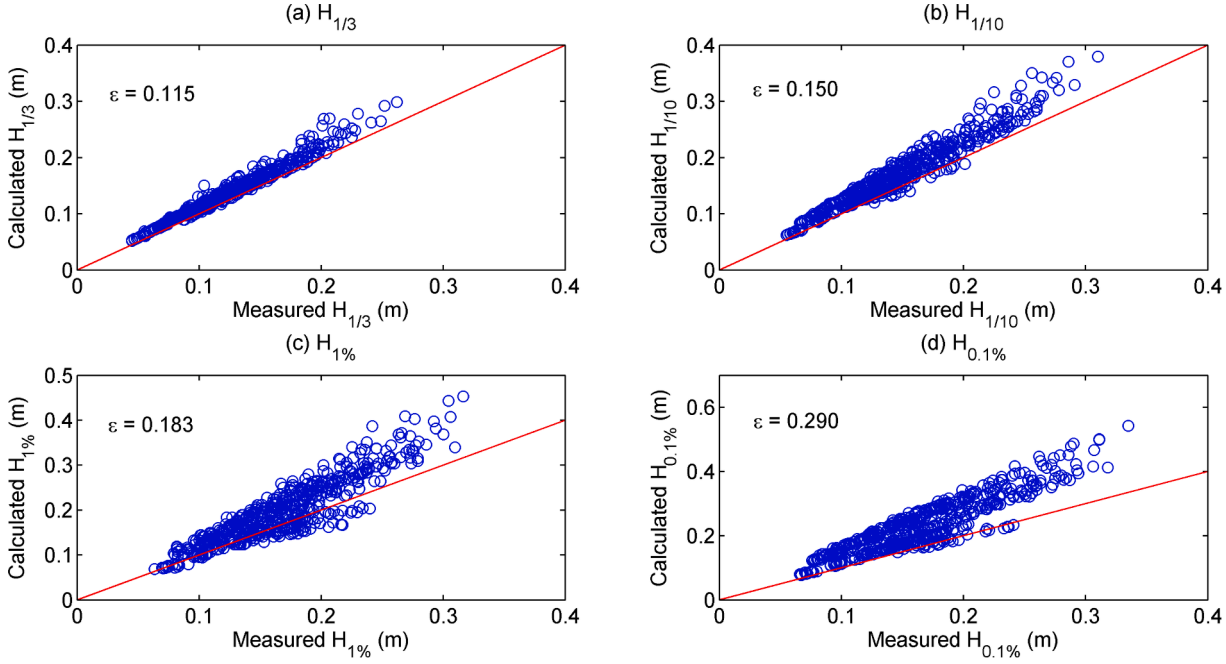

Fig. 14. Characteristic wave heights predicted by the BG 2000 (Battjes and Groenendijk, 2000) compared with measurements: (a) $H_{1/3}$ (b) $H_{1/10}$ (c) $H_{1\%}$ (d) $H_{0.1\%}$.

Table 2
Existing datasets for model validations.

Project	Fore-reef slope	Number of test cases	m_0 (10^{-4}m^2)	$\sqrt{m_0}/d$	Number of waves N
Tuan and San (2018)	1/8–1/20	4	3.03–4.57	0.116 - 0.214	1000
Anh (2018)	1/25	25	1.81- 16.3	0.067- 0.150	650

and from the measurements, respectively, N_p is the number of data points.

Overall, all characteristic wave heights are well-predicted by the 3WD (small errors $\varepsilon = 6\%$ - 11%). In particular, the estimates of average-based wave heights $H_{1/3}$ and $H_{1/10}$ are slightly better than those of extreme exceedance probabilities $H_{1\%}$ and $H_{0.1\%}$. As expected, the BG2000 generally overestimates all considered characteristic wave heights (i.e. data points largely stay above the straight line denoting the equivalence between model predictions and measurements), in which the predictions of extreme wave heights $H_{1\%}$ and $H_{0.1\%}$ are particularly worse ($\varepsilon = 18.3$ and 29.0%, respectively).

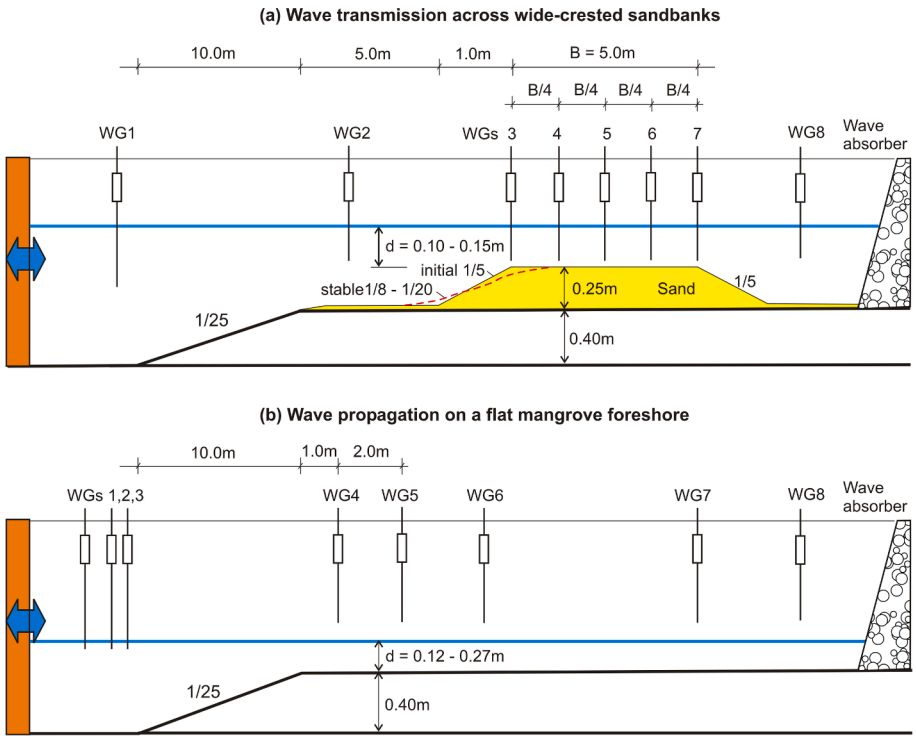

Fig. 15. Experimental setups: (a) wave transmission across a wide-crested sandbank (b) Wave propagation on a flat mangrove foreshore.

4.2. Model validation

The 3WD are validated against two existing laboratory datasets as outlined in Table 2, which include wave transmission across wide-crested sandbanks by Tuan and San (2018) and wave propagation on a shallow mangrove foreshore by Anh (2018). The aims of these experiments were originally different, however, these are considered suitable for model validations herein because of the resemblance in wave breaking conditions induced by the abrupt depth transition.

In the first case the model sandbank of 0.25 m in height and 5.0 m in

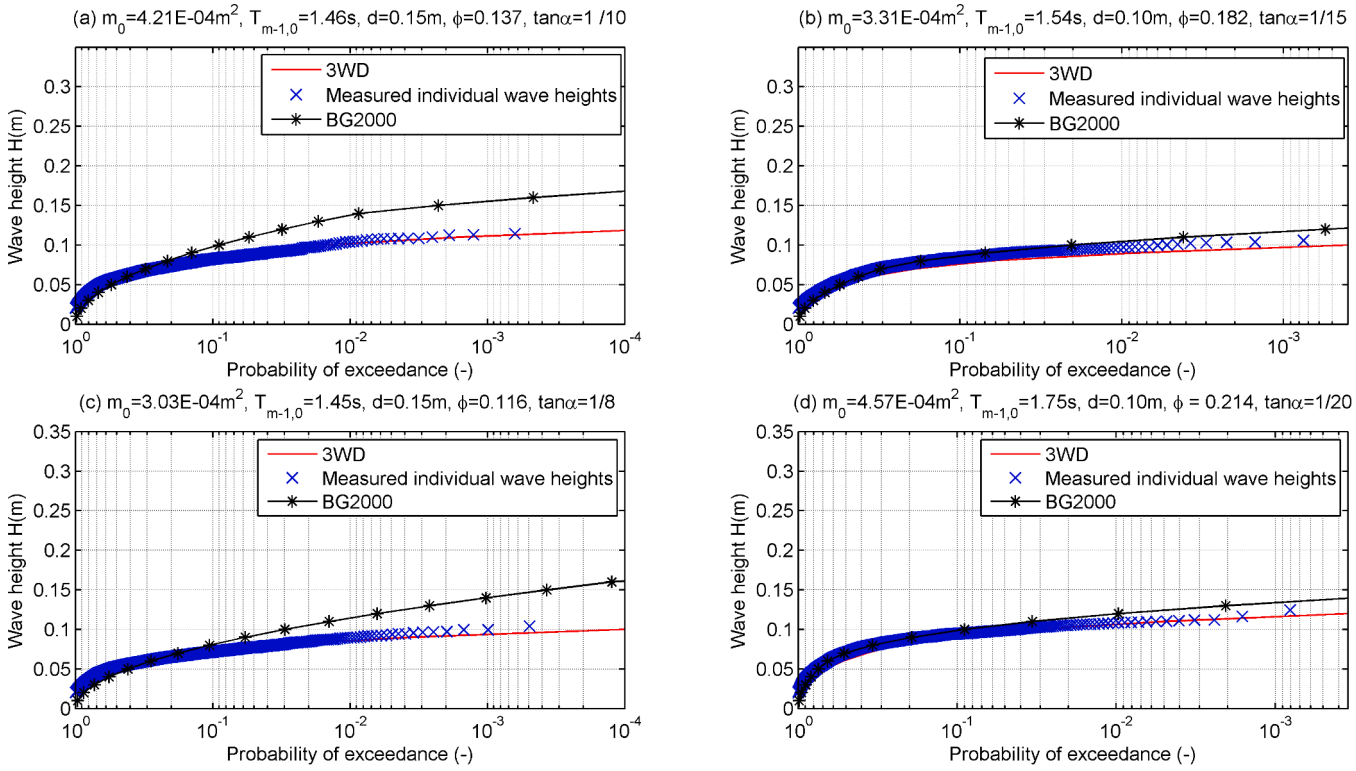

Fig. 16. Model validation, wide-crested sandbanks - wave height distributions with various fore-reef slopes: (a) tan$\alpha = 1/10$ (b) tan$\alpha = 1/15$ (c) tan$\alpha = 1/8$ (d) tan$\alpha = 1/20$.

crest width (B) was placed on a foreshore as illustrated in Fig. 15a. The seaward slope of the bank was 1/5 initially and became on average 1/8 to 1/20 after testing. Each of the test cases lasted for approximately 3000 waves. The deformation of the bank profile was mainly observed on the seaward slope and quickly evolved toward an equilibrium state just after the first 1000 waves. Herein, wave parameters are therefore based on the last 1000 waves only, over which the bank profile change is negligibly small. To further suppress the effect of local bed changes only the station WG5 at the middle of the bank is selected for consideration. The measured individual wave heights together with the corresponding distribution graphs by both the 3WD and the BG2000 model for four different test cases are shown in Fig. 16. It follows that the 3WD agrees well with the measurements in all test cases with the fore-reef slope ranging from steep to relatively gentle, which also affirms that the 3WD is rather insensitive to the change of the fore-reef slope. On the contrary, the predictions by the BG2000 model appears rather sensitive to the change of the local bed slope and are satisfactory in the case of gentle fore-reef slope only ($\tan\alpha = 1/15$ and 1/20, Fig. 16b and d).

In a similar setting but without the sandbank, Anh (2018) carried out a series of experiments on wave transmission across a mangrove forest. To create wave breaking on a relatively flat foreshore (the same foreshore as used in the previous case) a transitional slope of 1/25 was introduced (see Fig. 15b). In fact the bed topography turns out to resemble that of a shallow fringing reef. Herein only the measurements at the location WG4 close to the reef edge (to minimize possible effects of wave setup) in the case without mangroves are considered. The predictions of common characteristic wave heights $H_{1/3}$, $H_{1/10}$, $H_{1\%}$ and H_N (as $N < 1000$, the largest wave height in N waves H_N is considered instead of $H_{0.1\%}$) by both the 3WD and the BG2000 model in comparison with the measured data are shown in Fig. 17. The relative mean-square errors by both models are also given (ε_{3WD} and ε_{BG} correspond to the errors by 3WD and the BG 2000, respectively). There is general agreement by both models, but in detail the 3WD under-predicts and the BG2000 model over-predicts the measured wave heights systematically. These discrepancies in part can be attributed to the different wave hydrodynamics on the fringing reef with the enhancement of wave setup and particularly potential resonant amplification of standing IG waves (see also Section 5). Overall, the predictive performance by the BG2000 model is slightly better (say about 6% more accurate) in this case. This is logical since the fore-reef slope of 1/25 is sufficiently mild as a beach slope, on which the BG2000 model but not the 3WD is most appropriate.

5. Discussion

IG waves have been realized as one of the important hydrodynamic features on steep reef environments as they are considerably enhanced relative to open gentle beaches. As a result, the presence of IG waves may play a role in altering the statistical properties of wave heights on the reef flat, suggesting the need for a more appropriate wave height distribution model as proposed in the present study. In this section, we look at the relevant characteristics of IG wave dynamics on platform reefs as observed from the experiments and subsequently address its possible effects on the distribution of wave heights. For this, it is also concerned with wave reflection because of its important connection with reef wave heights in general and with the dynamics of IG waves in particular. It is worth mentioning that reflection and IG waves are inherent to steep reefs and their effects have implicitly been incorporated in the formulations of wave height distribution model addressed in the previous sections.

5.1. Effects of wave reflection

In addition to modifying total wave heights, reflection of out-going IG waves at the seaward reef edge can entrap wave energy, leading to potential resonant amplification of standing IG waves on the reef flat (Nwogu and Demirbilek, 2010; Pomeroy et al., 2012; Buckley et al., 2018).

In the present experiments, wave reflection can occur at the fore-reef slope as well as at the riprap slope behind the reef. With reference to a platform reef in the field, reflection due to the fore-reef slope is an

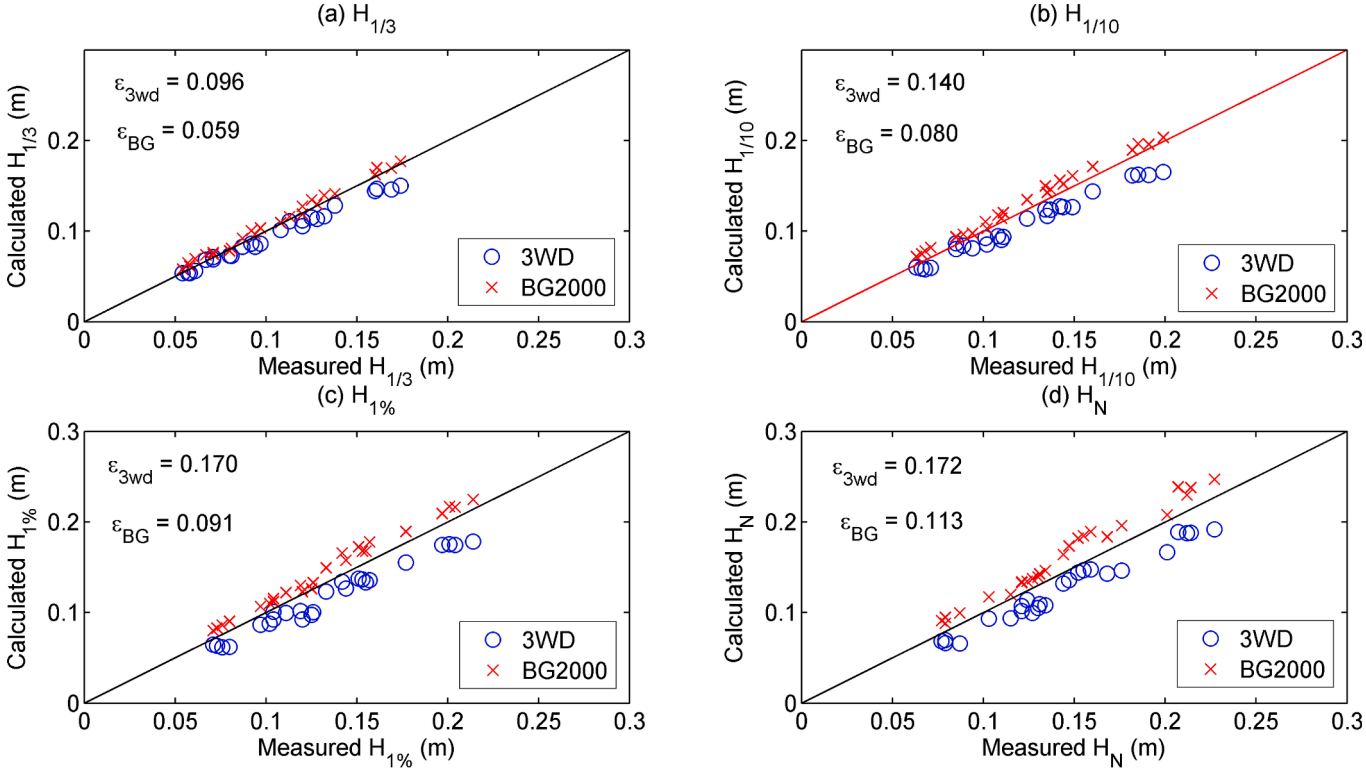

Fig. 17. Model validation, mangrove foreshore: (a) $H_{1/3}$ (b) $H_{1/10}$ (c) $H_{1\%}$ (d) H_N.

intrinsic manner, whilst that due to the riprap slope is considered as laboratory effects (though without the back-reef slope waves are still reflected due to a rapid change in wave celerity when leaving from the reef flat to a deeper region).

For the evaluation of the effect of wave reflection on wave heights, it is presumed that linear wave theory is still adequate for describing the across-shore energy flux of progressive waves over the reef flat (see e.g. Pomeroy et al., 2012; Yao et al., 2013; Buckley et al., 2018). Also, because the reef surface in this study is smooth, the effect of bottom friction can be ignored. The conservation equation of wave energy within a cell between an offshore point and a point on the reef flat is according to:

$$E_0\left(1-K_{R,0}^2\right)c_{g,0}=E_i\left(1-K_{R,i}^2\right)c_{g,i}+D_b \tag{21}$$

where $E=1/8\rho g H^2_{rsm}$ is the wave energy density, c_g is the group velocity, ρ is the water density, g is the acceleration of gravity, D_b is the time-averaged wave energy dissipation due to breaking within the considered section, K_R is the bulk reflection coefficient, the subscripts *0* and *i* denote quantities evaluated at locations offshore and on the reef flat, respectively. Note that reflection measured at a location on the reef flat ($K_{R,i}$) is mainly from the back-reef slope, whilst that measured at the offshore location ($K_{R,0}$) is from both the back-reef and the fore-reef slopes.

The energy dissipated by breaking D_b can be expressed in terms of local parameters (wave and water depth) according to a random wave breaking model such as by Battjes and Janssen (1978) or Thornton Guza (1983). Hence, Eq. (18) is further worked out with the expressions of E and D_b substituted:

$$\frac{1}{8}\rho g H_{rms,0}^2\left(1-K_{R,0}^2\right)c_{g,0}=\frac{1}{8}\rho g H_{rms,i}^2\left(1-K_{R,i}^2\right)c_{g,i}+\frac{1}{8}\rho g A_b f_p Q_b H_{rms,i}^2 \tag{22}$$

where f_p is a representative (peak) wave frequency, Q_b is the breaking fraction, and A_b is an intermediate model parameter.

Subsequently, the RMS wave height incorporating the effect of wave reflection for a location on the reef flat reads:

$$H_{rms,i}=\sqrt{\frac{\left(1-K_{R,0}^2\right)c_{g,0}}{\left(1-K_{R,i}^2\right)c_{g,i}+A_b f_p Q_b}}H_{rms,0} \tag{23}$$

The effect of wave reflection is further clarified through the ratio of the RMS wave height according to Eq. (20) to the one determined without reflection effects (i.e. $K_{R,0}=0$ & $K_{R,\mathrm{i}}=0$):

$$\delta_R=\sqrt{\frac{\left(1-K_{R,0}^2\right)\left(c_{g,i}+A_b f_p Q_b\right)}{\left(1-K_{R,i}^2\right)c_{g,i}+A_b f_p Q_b}} \tag{24}$$

$$\delta_{R,\max}=\sqrt{\left(1-K_{R,0}^2\right)} \tag{25}$$

where $\delta_R\le 1.0$ is the wave height reduction factor due to reflection. The reduction is largest (i.e. $\delta_R=\delta_{R,\max}$) when either reflection from the back-reef slope is minimal ($K^2_{R,i}\approx 0$) or the contributing effect from reflection is negligibly small compared to that from wave breaking (i.e. $K^2_{R,i}c_{g,i}\ll A_b f_p Q_b$).

Wave reflection at a location on the reef flat can be evaluated with the incoming and outgoing shore-normal energy fluxes determined from co-located spectra measured at that location (Sheremet et al., 2002). Unfortunately, synchronous velocity measurements at the wave gauge locations were not available. Therefore, reflection analysis is possible herein with the three-gauge array at the horizontal deep section only. Reflection coefficients at frequencies of interest are determined according to Zelt and Skjelbreia (1992), a generalised least-squares method of Mansard and Funke (1980) for an arbitrary number of wave gauges (see also Section 2). Wave spectra were split at half of the peak spectral frequency in each of the wave cases ($f_p/2$, see Table 1), for the determination of short-period (sea-swell) waves (SS, $f\ge f_p/2$) and IG waves ($0.025<f<f_p/2$).

Note that Eq. (18) and subsequently Eqs. (20) and (21) are valid for total wave heights with bulk reflection coefficients only (integrated over the full relevant frequency range including both SS and IG bands). Their use solely for either SS waves or IG waves may induce significant errors because of possible nonlinear energy transfers amongst different frequencies (see e.g. Henderson et al., 2006; Pomeroy et al., 2012). Herein, bulk reflection coefficients are used in Eqs. (21) and (22) for assessing the overall effect of wave reflection on the RMS wave height (and thus on the wave height distribution). Reflection of IG waves is more relevant for addressing the dynamics of IG waves and its subsequent influences (see Section 5.2).

Fig. 18 presents variations of the reflection coefficient measured at the offshore location with the relative reef-flat submergence $d/H_{m0,0}$ (with $H_{m0,0}$ being the incoming offshore wave height) for the total waves (bulk coefficient, K_R), short-period waves ($K_{R,SS}$), and IG waves ($K_{R,IG}$), respectively. It appears that both the bulk reflection coefficient and the reflection coefficient of SS waves are relatively small (K_R & $K_{R,SS}=0.07$–0.19) and both clearly increase with decreasing relative reef-

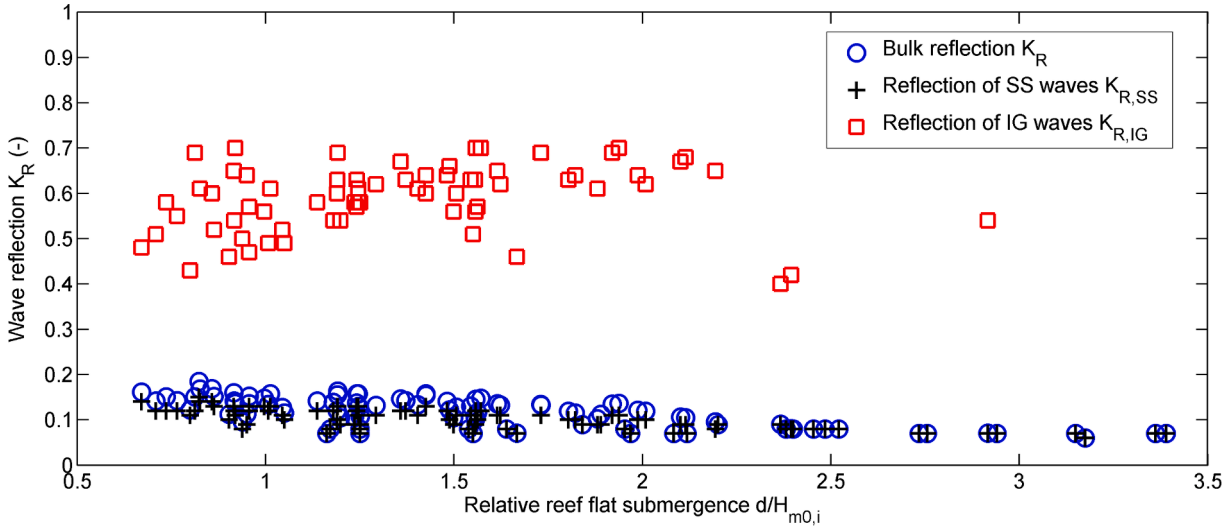

Fig. 18. Reflection coefficients at deep offshore section: total waves (circles), SS waves (plus signs), IG waves (squares).

flat submergence. Reflection from the riprap slope can be examined when the relative reef-flat submergence $d/H_{m0,0}$ is sufficiently large such that the effect of the fore-reef slope is minimal. It can be seen from Fig. 18 that when $d/H_{m0,0} > 2.70$ the bulk reflection coefficient becomes very small ($K_R = 0.07$), which is largely due to the riprap slope alone. Conversely, highest reflection occurs at low water levels (i.e. $K_R = 0.19$ when $d/H_{m0,0} < 1.5$) and is mostly generated on the fore-reef slope. As expected, highest reflection is observed for IG waves with $K_{R,\,IG}$ varying in the range from 0.40 to 0.70. No clear dependence of IG waves reflection on the relative reef-flat submergence is observed.

With the highest reflection coefficient measured at the offshore boundary $K_{R,0} = 0.19$ (Fig. 18) and given a minimal reflection from the back-reef slope ($K_{R,i} \approx 0$), the largest reduction of the RMS wave height can be estimated according to Eq. (22), which is only about 2.0% ($\delta_{R,\,\max} \approx 0.98$). This is within the measurement error for wave heights. Therefore, the effect of wave reflection on the RMS wave height and consequently on the distribution of wave heights in the present study is negligible.

5.2. Effects of infra-gravity waves

At first, wave reflection is also important to the dynamics of IG waves. At the deep offshore section, the incoming IG wave height is very small (since IG waves are mostly generated inside the surfzone) whilst the outgoing IG wave height is relatively large, hence the reflection coefficient of IG waves at this location is highest over the entire reef flat (see also Buckley et al., 2018). In other words, the reflection coefficients of IG waves at a specific location on the reef flat would not exceed 0.70 (or $K^2_{R,IG} < 0.50$, see also Fig. 18), implying that IG waves are predominantly shoreward progressive throughout the reef flat. As a consequence, partial standing or standing IG waves could not exist and resonant amplification of IG waves on the reef flat did not occur.

Without loss of generality, Fig. 19 presents variations of the spectral wave height of SS ($H_{m0,SS}$) and IG ($H_{m0,IG}$) waves at various locations across the reef, for two representative cases of lowest and highest water depths on the reef flat under the same high offshore incident wave (fore-reef slope $\tan\alpha = 1/5$, water depth: $d = 0.15$ m and 0.40 m, offshore wave: $H_{m0,0} = 0.20$ m and $T_p = 1.80$s). In both cases, the SS wave height $H_{m0,SS}$ substantially reduces due to depth-induced breaking around the reef edge and gradually decreases behind the surfzone. However, SS waves are still the major component in the total wave energy across the reef flat, because of moderate breaking conditions associated with a relative large reef-flat submerged depth considered in this study ($d/H_{m0,0} = 0.67$–3.46, see also Table 1).

The IG wave height $H_{m0,IG}$ initially peaks in the surfzone around the reef edge and subsequently decays over the remaining part of the reef at a much slower rate than SS waves (for example, due to IG energy transfer back to higher frequencies, see also Henderson et al., 2006). Although with a very small proportion in the total wave height in deep water, the relative importance of IG waves becomes more significant as waves propagates over the reef flat, particularly for the case of low water level (for the case of small water depth in Fig. 19a, the ratio $H_{m0,IG}/H_{m0,SS}$ increases from 0.12 in deep water to 0.31 around the reef edge, and reaches the maximum value of 0.34 at a location on the inner reef flat; these corresponding values are 0.12, 0.14, and 0.18 for the case of large water depth in Fig. 19b).

Overall, the characteristics of IG waves transformation over the reef as observed from the present experiments agree well with the preceding laboratory works such as by Nwogu and Demirbilek (2010), and Buckley et al. (2018). However, herein, the IG wave height is considerably smaller than the SS wave height and the wave hydrodynamics across the reef, also because of no potential IG wave resonance, is overwhelmingly dominated by SS waves.

The existing models of the wave height distribution on shallow beaches (Glukhovskiy, 1966; Klopman, 1996; Battjes and Groenendijk, 2000) mainly focus on the deviation of extreme (highest) waves in the tail of the distribution ascribed to effects of depth-induced wave breaking. Possible departure of the statistical properties of lower wave heights, however, is unclear or ignored, albeit these waves are most related to effects that are enhanced in shallow water such as nonlinearities and finite spectral bandwidth.

As shown earlier, the proportion of IG waves in the total wave energy becomes more significant on the reef flat, implying that wave nonlinearities may cause the distribution of lower waves to differ significantly from the Rayleigh one. The evidence can be seen from the analysis in Section 3 (Figss. 2–4) that the middle part of the distribution with intermediate wave heights (including IG waves) evolves markedly with the local conditions. Effects of IG waves are therefore most

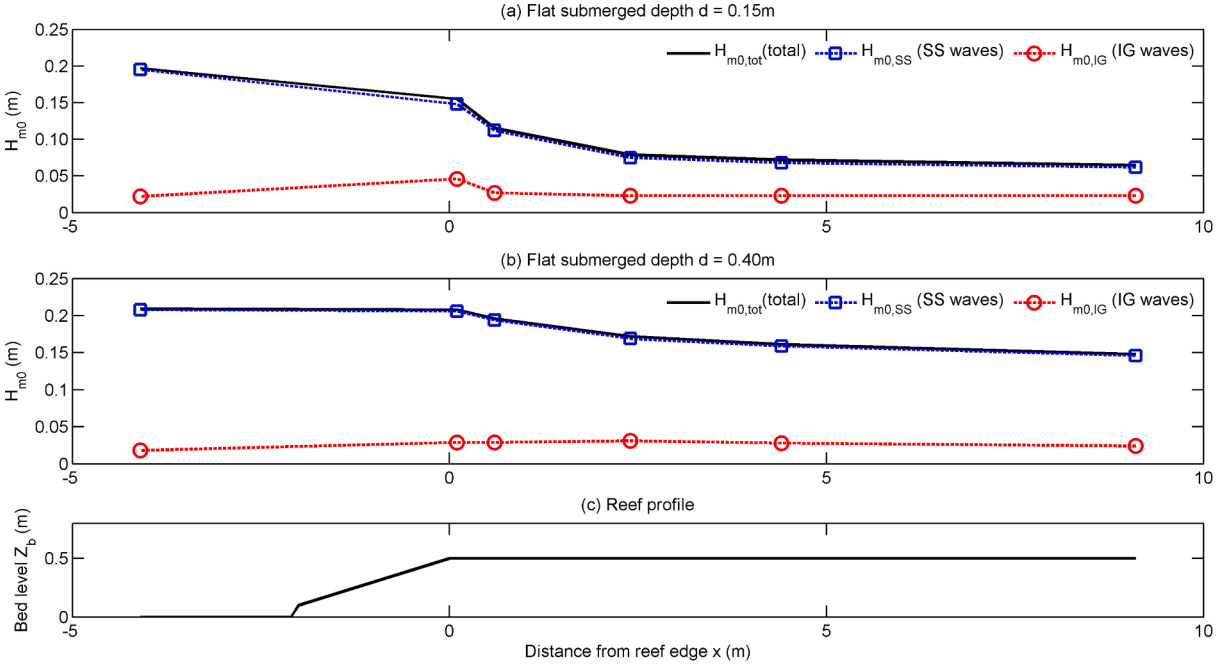

Fig. 19. Across-reef transformation of SS and IG waves: (a) Low reef water depth $d = 0.15$ m (b) High reef water depth $d = 0.40$ m (c) Reef profile.

exhibited in the mid part of the distribution (i.e. the second Weibull part) in the present study. As noted in Subsection 3.3 that the ratio $H_{rms}/\sqrt{m_0}$ gets higher as waves become more nonlinear in shallow water. Herein, effects of IG waves can therefore be interpreted via their nonlinearities causing the increase of the ratio $H_{rms}/\sqrt{m_0}$ with increasing relative wave intensity ϕ on the reef flat (Eq. (13) and Fig. 10), which consequently tends to increase the heights of intermediate waves in the middle part of the distribution (see Fig. 2a–c). Overall, the effect of IG waves has also been accounted for in the 3WD through the use of the characteristic spectral period $T_{m-1,0}$ in the model parameterization (see Subsection 3.3).

Finally, it is worthwhile to mention about the applicability range of the 3WD presented in this study. The derived model parameters are valid for hydraulic conditions satisfying the range of tested conditions as follows: $\sqrt{m_0}/d = 0.06–0.26$, $d/L_{0m} = 0.01–0.19$, $d/H_{m0,0} = 0.67–3.46$. Also, albeit the model parameterization is based on tested cases with two steep fore-reef slopes only ($\tan\alpha = 1/5$ and $1/10$), it is evidenced from the above model validations that the validity of the 3WD goes beyond this slope limit and is still reliable for fore-reef slopes as mild as 1/20. The 3WD has been formulated with the laboratory wave data on platform reefs with the dominance of sea-swell (short-period) waves. To what extent the new distribution model can be applied to fringing reefs, particularly at locations with the dominance of IG waves due to resonant amplification, has not been investigated.

6. Conclusions

The present paper is concerned with a laboratory study on the distribution of wave heights on steep platform reefs. It is experimentally shown that existing models incorporating the effect of wave breaking on a shallow beach fail to reliably describe the wave height distribution on the shallow reef flat. This is due to the fact that wave breaking and nonlinearity induced by sudden depth reduction over a steep fore-reef slope might differ substantially from those induced by gradual depth variation on a gently-sloping shallow beach. In addition to the local relative wave intensity, the wave height distribution is found to complexly depend on the reef-flat shallowness and on the fore-reef slope. A new composite distribution, which extends the approach by Battjes and Groenendijk (2000), is therefore proposed. The new model is generally composed out of three Weibull parts and collapses to a two-Weibull one when the relative wave intensity drops below a critical level. The model parameters are formulated as functions of the local input parameters through least-square fitting all individual wave heights from 540 measured wave records at various locations across the reef flat. The experimental data on most common characteristics wave heights and the model predictions are found in very good agreement. The model is validated against two existing laboratory datasets of wave heights on reefs with various fore-reef slopes, showing that good model predictive capacity is found for fore-reef slopes steeper than 1/20. Further studies on model validations against field datasets and on effects of various reef morphology are recommended.

References

Anh, N.T., 2018. Wave Attenuation across Shallow Coastal Mangrove Forests (In Vietnamese). PhD dissertation. Vietnam Academy for Water Resources Research, 150pp.

W.L., 2004. DELFT-AUKEPC reference manual. DELT HYDRAULICS, p. 142pp.

Battjes, J.A., 1974. Surf similarity. In: Proceedings of the 14th International Conference on Coastal Engineering. ASCE, pp. 466–480.

Battjes, J.A., Groenendijk, H.W., 2000. Wave height distributions on shallow foreshores. Coast Eng. 40, 161–182.

Battjes, J.A., Janssen, J.P.F.M., 1978. Energy loss and set-up due to breaking of random waves. In: Proc. 16th International Conference on Coastal Engineering. ASCE, pp. 569–588.

Becker, J.M., Merrifield, M.A., Yoon, H., 2016. Infra-gravity waves on fringing reefs in the tropical Pacific: dynamic setup. J. Geophys. Res.: Oceans 121, 3010–3028.

Boers, M., 1996. Simulation of a Surf Zone with a Barred Beach, Part 1: Wave Heights and Wave Breaking. Communication on Hydraulic and Geotechnical Engineering. Report no. 96-5. Delft University of Technology, Delft, The Netherlands.

Bouws, E., 1979. Spectra of extreme wave conditions in the Southern North Sea considering the influence of water depth. In: Proceedings Conference on Sea Climatology: Collection Colloquia at Seminars, vol. 34, pp. 51–69.

Buckley, M.L., Lowe, R.J., Hansen, J.E., van Dongeren, A.R., 2015. Dynamics of wave setup over a steeply sloping fringing reef. J. Phys. Oceanogr. 45, 3005–3023.

Buckley, M.L., Lowe, R.J., Hansen, J.E., van Dongeren, A.R., 2016. Wave setup over a fringing reef with large bottom roughness. J. Phys. Oceanogr. 46, 2317–2333.

Buckley, M.L., Lowe, R.J., Hansen, J.E., van Dongeren, A.R., Storlazzi, C.D., 2018. Mechanisms of wave-driven water level variability on reef-fringed coastlines. J. Geophys. Res.: Oceans 123.

Caires, S., van Gent, M.R.A., 2012. Wave height distribution in constant and finite depths. In: Proceedings of the 33rd International Conference on Coastal Engineering. ASCE, p. 33.

Christou, M., Rijnsdorp, D.P., Ewans, K., 2011. Analysis of shallow water wave measurements recorded at the Field Research Facility. In: Proceedings of 12th International Workshop on Wave Hindcasting & Forecasting & 3rd Coastal Hazards Symposium, 12pp.

Dally, W.R., Dean, R.G., 1986. Transformation of random breaking waves on surf beat. In: Proceedings of 20th International Conference on Coastal Engineering, pp. 109–123.

Demirbilek, Z., Nwogu, O.G., Ward, D.L., 2007. Laboratory study of wind effect on runup over fringing reefs. Report 1: Data report. In: Coastal and Hydraulics Laboratory Technical Report ERDC/CHL-TR-07-4. U.S. Army Engineer Research and Development Center, Vicksburg, MS, p. 84.

EurOtop, Van der Meer, J.W., 2018. In: Allsop, N.W.H., Bruce, T., De Rouck, J., Kortenhaus, A., Pullen, T., Schüttrumpf, H., Troch, P., Zanuttigh, B. (Eds.), Manual on wave overtopping of sea defences and related structures. An overtoppingmanual largely based on European research, but for worldwide application, second ed. www.overtopping-manual.com

Glukhovskiy, B. Kh, 1966. Issledovaniye Morskogo Vetrovogo Volneniya (Investigation of Sea Waves). Gidrometeoizdat, Leningrad (in Bouws, 1979).

Gourlay, M.R., 1994. Wave transformation on a coral reef. Coast. Eng. 23, 17–42.

Gourlay, M.R., 1996. Wave set-up on coral reefs. 2. Set-up on reefs with various profiles. Coast Eng. 28, 17–55.

Gourlay, M.R., 1996. Wave set-up on coral reefs. 1. Set-up and wave-generated flow on an idealized two dimensional horizontal reef. Coast Eng. 27, 161–193.

Groenendijk, H.W., van Gent, M.R.A., 1998. Shallow Foreshore Wave Height Statistics: a Predictive Model for the Probability of Exceedance of Wave Heights. Delft Hydraulics report No, p. H3351.

Henderson, S.M., Guza, R.T., Elgar, S., Herbers, T.H.C., Bowen, A.J., 2006. Nonlinear generation and loss of infragravity wave energy. J. Geophys. Res. 111, C12007.

Hofland, B., Chen, X., Altomare, C., Oosterlo, P., 2017. Prediction formula for the spectral wave period $T_{m-1,0}$ on mildly sloping shallow foreshores. Coast Eng. 123, 21–28.

Huang, Z.C., Lenain, L., Melville, W.K., Middleton, J.H., Reineman, B., Statom, N., McCabe, R.M., 2012. Dissipation of wave energy and turbulence in a shallow coral reef lagoon. Journal of Geophysical Research-Oceans 117, C03015.

Klopman, G., 1996. Extreme Wave Heights in Shallow Water, Report H2486. WL/Delft hydraulics, The Netherlands.

Longuet-Higgins, M.S., 1952. On the statistical distributions of heights of sea waves. J. Mar. Res. 11, 245–266.

Lowe, R.J., Falter, J.L., Bandet, M.D., Pawlak, G., Atkinson, M.J., Monismith, S.G., 2005. Spectral wave dissipation over a barrier reef. J. Geophys. Res. 110, C04001.

Mai, S., Wilhelmi, J., Barjenbruch, U., 2010. Wave height distributions in shallow waters. In: Proceedings of 32rd International Conference on Coastal Engineering, p. 32, 6 pp.

Mansard, E.P.D., Funke, E.R., 1980. The measurement of incident and reflected spectra using a least squares method. In: Proceedings of 17th International Conference on Coastal Engineering, pp. 154–172.

Mase, H., Iwagaki, M., 1982. Wave height distributions and wave grouping in the surf zone. In: Proceedings of 18th International Conference on Coastal Engineering. ASCE, pp. 58–76.

Miche, R., 1944. Mouvements ondulatoires de la mer en profondeur constante ou decroissante forme limite de la houle lors de son deferlement. Annales des Ponts et Chaussees, pp. 285–319.

Nakaza, E., Hino, M., 1991. Bore-like surf beat in a reef zone caused by wave groups of incident short-period waves. Fluid Dyn. Res. 7, 89–100.

Nelson, R.C., 1994. Depth limited design wave heights in very flat regions. Coast Eng. 23, 43–59.

Nwogu, O., Demirbilek, Z., 2010. Infragravity wave motions and runup over shallow fringing reefs. J. Waterw. Port, Coast. Ocean Eng. 136, 295–305.

Péquignet, A.C.N., Becker, J.M., Merrifield, M.A., Aucan, J., 2009. Forcing of resonant modes on a fringing reef during tropical storm Man-Yi. Geophys. Res. Lett. 36, L03607.

Pomeroy, A., Lowe, R., Symonds, G., Dongeren, A.V., Moore, C., 2012. The dynamics of infragravity wave transformation over a fringing reef. J. Geophys. Res. 117, C11022.

Rattanapitikon, W., 2010. Verification of conversion formulas for computing representative wave heights. Ocean Eng. 37, 1554–1563.

Sheremet, A., Guza, R.T., Elgar, S., Herbers, T.H.C., 2002. Observations of nearshore infragravity waves: seaward and shoreward propagating components. J. Geophys. Res. 107 (C8), 3095.

Tayfun, M.A., 1981. Breaking-limited wave heights. J. Waterw. Port, Coast. Ocean Eng. 107 (2), 59–69.

Thornton, E.B., Guza, R.T., 1983. Transformation of wave height distribution. J. Geophys. Res. 88, 5925–5938.
Tuan, T.Q., San, D.C., 2018. Large-scale nourishment by near-shore sandbanks for erosion controlof mangrove mud coasts: a laboratory study on cross-shore processes. In: Proceedings of Vietnam International Water Week VACI2018, Hanoi, Vietnam.
Tuan, T.Q., Tien, N.V., Verhagen, H.J., 2016. Wave transmission over submerged, smooth and impermeable breakwaters on a gentle and shallow foreshore. In: Proceedings of 9-th PIANC-COPEDEC, pp. 897–905 (Rio de Janeiro, BRAZIL).
Van Gent, M.R.A., 2001. Wave run-up on dikes with shallow foreshores. J. Waterw. Port, Coast. Ocean Eng. 127, 5.
Vasiliki, K., Swan, C., 2011. An experimental study of shallow water wave statistics on mild bed slopes. In: Proceedings of 30th International Conference on Ocean, vol. 2. Offshore and Arctic Engineering, pp. 711–719.
Vledder, G.P., Ruessink, G., Rijnsdorp, D., 2013. Individual wave height distributions in the coastal zone: measurements and simulations and the effect of directional spreading. Coastal Dynamics 1799–1810.
Wu, Y., Randell, D., Christou, M., Ewans, M., Jonathan, P., 2016. On the distribution of wave height in shallow water. Coast Eng. 111, 39–49, 2016.
Yao, Y., Huang, Z.H., Monismith, S.G., Lo, E.Y.M., 2013. Characteristics of monochromatic waves breaking over fringing reefs. J. Coast. Res. 29, 94–104.
Yao, Y., Zhang, Q.M., Chen, S.G., Tang, Z.J., 2019. Effects of reef morphology variations on wave processes over fringing reefs. Appl. Ocean Res. 82, 52–62.
Zelt, J.A., Skjelbreia, J.E., 1992. Estimating incident and reflected wave fields using an arbitrary number of wave gauges. In: Proceedings of 23rd International Conference on Coastal Engineering. ASCE, pp. 777–789.